A non-overlapping domain decomposition method with perfectly matched layer transmission conditions for the Helmholtz equation

Anthony Royer[a], Christophe Geuzaine[a,*], Eric Béchet[b], Axel Modave[c]

[a] *Université de Liège, Institut Montefiore, All. de la Découverte 10, 4000, Liège, Belgium*
[b] *Université de Liège, Département Aérospatial et Mécanique, All. de la Découverte 9, 4000, Liège, Belgium*
[c] *POEMS, CNRS, Inria, ENSTA Paris, Institut Polytechnique de Paris, 828 Bd. des Maréchaux, 91120, Palaiseau, France*

Abstract

It is well-known that the convergence rate of non-overlapping domain decomposition methods (DDMs) applied to the parallel finite-element solution of large-scale time-harmonic wave problems strongly depends on the transmission condition enforced at the interfaces between the subdomains. Transmission operators based on perfectly matched layers (PMLs) have proved to be well-suited for configurations with layered domain partitions. They are shown to be a good compromise between basic impedance conditions, which lead to suboptimal convergence, and computational expensive conditions based on the exact Dirichlet-to-Neumann (DtN) map related to the complementary of the subdomain. Unfortunately, the extension of the PML-based DDM for more general partitions with cross-points (where more than two subdomains meet) is rather tricky and requires some care.

In this work, we present a non-overlapping substructured DDM with PML transmission conditions for checkerboard (Cartesian) decompositions that takes cross-points into account. In such decompositions, each subdomain is surrounded by PMLs associated to edges and corners. The continuity of Dirichlet traces at the interfaces between a subdomain and PMLs is enforced with Lagrange multipliers. This coupling strategy offers the benefit of naturally computing Neumann traces, which allows to use the PMLs as discrete operators approximating the exact Dirichlet-to-Neumann maps. Two possible Lagrange multiplier finite element spaces are presented, and the behavior of the corresponding DDM is analyzed on several numerical examples.

Keywords: Finite elements, Domain decomposition, Helmholtz equation, Cross-points, Perfecly matched layer, Transmission condition

1. Introduction

Large-scale time-harmonic wave problems need to be solved in many application areas, such as acoustic, seismic and medical imaging, ground characterization or electromagnetic compatibility. Such wave propagation problems remain a very challenging issue in engineering, especially in the high-frequency regime, when the wavelength is much smaller than the geometrical dimensions of the domain of study. Among the various approaches that can be used to solve large-scale time-harmonic wave problems, the Finite Element Method (FEM) is widely used for its ability to handle complex geometrical configurations and materials with non-homogeneous properties.

Because of the highly oscillatory nature of the wave fields, the brute-force application of the FEM leads to a large number of unknowns and a poorly-conditioned complex-valued linear system [45]. Direct solvers do not scale well for such problems and Krylov subspace iterative solvers exhibit slow convergence or can even diverge, while efficiently preconditioning proves difficult [24]. Domain decomposition methods (DDMs) provide an interesting alternative. These methods rely on a partition of the computational domain into subdomains, and an iterative procedure using subproblems of smaller sizes, amenable to sparse direct solvers

*Corresponding author
Email addresses: anthony.royer@uliege.be (Anthony Royer), cgeuzaine@uliege.be (Christophe Geuzaine), eric.bechet@uliege.be (Eric Béchet), axel.modave@ensta-paris.fr (Axel Modave)

(see *e.g.* [63]). For acoustic time-harmonic wave problems, governed by the scalar Helmholtz equation, a recent overview of DDMs can be found in [31]. Among all DDMs, we can highlight Schwarz methods with overlap [12, 30, 38] or without overlap [4, 16, 32], FETI algorithms [19, 25–27] and the method of polarized traces [65, 66], which are eventually combined with preconditioning techniques (see *e.g.* [18, 33, 35, 58, 59, 64]).

In this work, we focus on Schwarz-type domain decomposition algorithms without overlap of the subdomains. The convergence rate of these methods strongly depends on the transmission condition enforced on the interfaces between the subdomains. The optimal convergence is obtained by imposing the Dirichlet-to-Neumann (DtN) map related to the complementary of each subdomain [46, 47]. For acoustic waves, this DtN map links the Dirichlet trace of the pressure field on the interface to its normal derivative, which corresponds to the normal displacement. Since the cost of computing the exact DtN is prohibitive, operators based on low-order absorbing boundary conditions (ABCs) to approximate the DtN have been developed since the late 80's and early 90's [20, 36, 48], followed in the late 90's and early 00's by (optimized) second-order transmission conditions [32, 54]. More recently, domain decomposition strategies were developed with high-order transmission conditions [10, 11, 37, 42], transmission conditions based on perfectly matched layers (PMLs) [58, 64] and non-local transmission operators [17, 39, 40, 60]. In a general way, high-order and PML-based conditions accelerate the convergence of DDMs in comparison with low-order conditions, with an extra cost per iteration that can be controlled thanks to the order of the conditions or the thickness of the PMLs. Non-local approaches are more expensive per iteration in term of computational cost, but they have the best convergence rate and a strong theoretical background is available [16, 17, 39].

Most of the DDMs with high-order, PML-based and non-local transmission operators have initially been tested and studied for configurations with one-dimensional domain partitions (*e.g.* layered partitions, partitions of spherical shells into onion peels, ...). Such partitions do not exhibit (interior) cross-points (*i.e.* points where more than two subdomains meet), which simplifies the implementation and avoids technical difficulties with the transmission conditions. However, for large-scale two- and three-dimensional applications, one-dimensional partitions are not optimal, as the amount of data to transfer between the subdomains can be far smaller with multi-dimensional partitions (*e.g.* Cartesian and checkerboard partitions, general partitions generated with automatic mesh partitioners, ...). With such partitions, the cross-points require some care, especially when transmissions conditions with differential or integral operators are used. Specific strategies to deal with cross-points have been proposed for DDMs with low-order transmission conditions and nodal finite element discretizations (*e.g.* [5, 27, 29]). Recently, cross-point treatments have been proposed for DDMs with second-order conditions [21, 28, 51] and non-local approaches [13–15, 22, 52] in order to address general domain partitions. In the case of high-order (Padé-type) transmission conditions, a cross-point treatment has been proposed in [44], by using corner compatibility relations developed for high-order absorbing boundary conditions (HABC) prescribed on the edges of rectangular domains [43]. This approach, which is limited to checkerboard partitions, proves to be very efficient and naturally deals with boundary cross-points (*i.e.* points where an interface meet an exterior border with an absorbing boundary treatment). To the best of our knowledge, non-overlapping (substructured) domain decomposition algorithms with PML-based transmission have been tested only for layered partitions [58, 64], and no cross-point treatment has been proposed yet to address checkerboard partitions. Let us mention that parallel domain decomposition preconditioners using PMLs at the border of the subdomains have been proposed with layered partitions [56, 62] and multi-dimensional partitions [1, 41], but these preconditioners do not require cross-point treatments.

In this article, we present a non-overlapping DDM with PML-based transmission conditions for two-dimensional Helmholtz problems. This method, designed for checkerboard domain partitions, takes naturally into account interior and boundary cross-points. PMLs are considered as operators imposed on interfaces through Lagrange multipliers. Two different discretization strategies for the Lagrange multipliers are studied.

The article is organized as follows. In Section 2 the Helmholtz problem is introduced on a rectangular domain, and the coupling with surrounding PMLs (*i.e.* four PMLs associated to the edges of the rectangle, and four PMLs associated to the corners) using Lagrange multipliers is presented. Two discretizations for the Lagrange multipliers are introduced, and the solvability and the stability of the resulting finite element problems are analyzed. Then, in Section 3, the DDM with PML-based transmission operators is introduced. The cross-point treatments are naturally taken into account through the PMLs used at the corners of the rectangular subdomains. In Section 4, some numerical examples are presented to analyze the behavior of the proposed methods. After an analysis of the influence of the PML parameters, the convergence of the

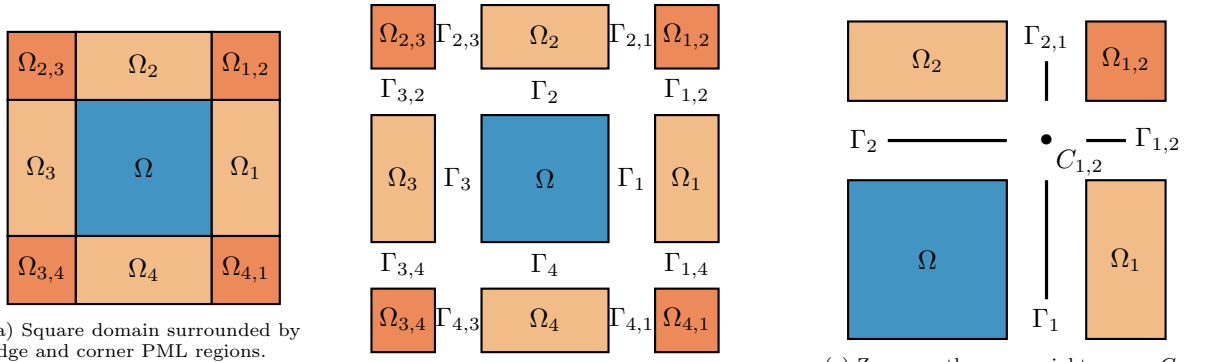

(a) Square domain surrounded by edge and corner PML regions.

(b) Coupling interfaces.

(c) Zoom on the upper right corner $C_{1,2}$.

Figure 1: A square domain Ω in blue with PML regions in orange.

domain decomposition algorithm is studied on representative finite element problems with homogeneous or heterogeneous media. Finally, conclusions and perspectives are proposed in Section 5.

2. Helmholtz problem with weakly-coupled PMLs

2.1. Definition of the problem

We consider a two-dimensional Helmholtz problem defined on a square domain Ω, which is surrounded with PML regions associated to the edges and the corners of Ω. These families of PML, respectively called edge PMLs and corner PMLs, are illustrated in Figure 1. The edges and the corners of Ω are denoted Γ_i (with $i = 1, \ldots, 4$) and $C_{i,j}$ (with $i, j = 1, \ldots, 4$, such that Γ_i and Γ_j are adjacent), respectively. The edge PML and corner PML associated to Γ_i and $C_{i,j}$ are denoted Ω_i and $\Omega_{i,j}$, respectively. The interface between a corner PML $\Omega_{i,j}$ and an edge PML Ω_i is denoted $\Gamma_{i,j}$. Let us note that $\Omega_{i,j} = \Omega_{j,i}$ but $\Gamma_{i,j} \neq \Gamma_{j,i}$. The exterior boundaries of the edge PMLs and the corner PMLs are denoted with Γ_i^{ext} and $\Gamma_{i,j}^{\text{ext}}$, respectively.

Denoting the union of the domain Ω, the edge PMLs and the corner PMLs as Ω_{all}, the global problem reads

$$\begin{cases} \operatorname{div}(\mathbb{D}\,\mathbf{grad}\,w) + Ek^2 w = -f, & \text{in } \Omega_{\text{all}}, \\ \mathbf{n}_{\text{all}} \cdot (\mathbb{D}\,\mathbf{grad}\,w) = 0, & \text{on } \partial\Omega_{\text{all}}, \end{cases} \tag{1}$$

where k is the (positive) wavenumber, the tensor field $\mathbb{D}(\mathbf{x})$ and the scalar field $E(\mathbf{x})$ are material properties, $f(\mathbf{x})$ is a source term, and $\partial_{\mathbf{n}_{\text{all}}}$ is the outgoing normal derivative. Inside the domain Ω, the material properties are $\mathbb{D} = \operatorname{diag}(1, 1)$ and $E = 1$, and they depend on absorption functions in the PML regions. The definition of $\mathbb{D}(\mathbf{x})$ and $E(\mathbf{x})$ in the PML regions is discussed in Section 4. The natural functional space for the global solution w is $H^1(\Omega_{\text{all}})$.

The global problem (1) can be rewritten as the coupling of nine subproblems associated to the square domain Ω and the edge/corner PML regions. The corresponding local solutions are denoted u, u_i and $u_{i,j}$, for Ω, Ω_i and $\Omega_{i,j}$, respectively. Let us note that $u_{i,j} = u_{j,i}$. The global solution w is simply obtained by combining these local solutions. The nine coupled subproblems read as follows:

- Subproblem associated to the square domain Ω:

$$\begin{cases} \Delta u + k^2 u = -f & \text{in } \Omega, \\ \partial_{\mathbf{n}} u = \mathbf{n} \cdot (\mathbb{D}_i\,\mathbf{grad}\,u_i) & \text{on each } \Gamma_i, \end{cases} \tag{2}$$

  where $\mathbf{n}$ is the outgoing normal with respect to Ω;

- Subproblems associated to each edge PML Ω_i (with $i = 1, \ldots, 4$):

$$\begin{cases} \operatorname{div}(\mathbb{D}_i \, \mathbf{grad}\, u_i) + E_i k^2 u_i = 0 & \text{in } \Omega_i, \\ \mathbf{n}_i \cdot (\mathbb{D}_i \, \mathbf{grad}\, u_i) = 0 & \text{on } \Gamma_i^{\text{ext}}, \\ u_i = u & \text{on } \Gamma_i, \\ \mathbf{n}_i \cdot (\mathbb{D}_i \, \mathbf{grad}\, u_i) = \mathbf{n}_i \cdot (\mathbb{D}_{i,j} \, \mathbf{grad}\, u_{i,j}) & \text{on each } \Gamma_{i,j}, \end{cases} \tag{3}$$

  where $\mathbf{n}_i$ is the outgoing normal with respect to Ω_i;

- Subproblems associated to each corner PML $\Omega_{i,j}$ (with $i, j = 1, \ldots, 4$ such that Γ_i and Γ_j are adjacent):

$$\begin{cases} \operatorname{div}(\mathbb{D}_{i,j} \, \mathbf{grad}\, u_{i,j}) + E_{i,j} k^2 u_{i,j} = 0 & \text{in } \Omega_{i,j}, \\ \mathbf{n}_{i,j} \cdot (\mathbb{D}_{i,j} \, \mathbf{grad}\, u_{i,j}) = 0 & \text{on } \Gamma_{i,j}^{\text{ext}}, \\ u_{i,j} = u_i & \text{on } \Gamma_{i,j}, \\ u_{i,j} = u_j & \text{on } \Gamma_{j,i}, \end{cases} \tag{4}$$

  where $\mathbf{n}_{i,j}$ is the outgoing normal with respect to $\Omega_{i,j}$.

In a nutshell, each local solution verifies the Helmholtz equation and a homogeneous Neumann condition on the exterior boundary (if any), and the coupling is performed by enforcing the continuity of the Dirichlet and Neumann traces at the interfaces.

2.2. Variational formulation with Lagrange multipliers

In the domain decomposition procedure, every rectangular subdomain of the checkerboard partition will be surrounded with edge and corner PMLs. The standard variational formulation based on System (1) could be used for each subproblem. However, the drawback of this approach lies in the lack of direct availability of the Neumann traces at the interfaces between each subdomain and the corresponding surrounding PMLs, while the domain decomposition procedure requires the knowledge of both Dirichlet and Neumann traces at these interfaces. In this work, we consider an alternative variational formulation based on the coupled systems (2), (3) and (4), where the continuity conditions at the interfaces are enforced by using Lagrange multipliers. This approach offers the benefit to naturally give access to the Neumann traces thanks to the Lagrange multipliers.

Let us introduce four *edge* Lagrange multipliers λ_i on the interfaces Γ_i (with $i = 1, \ldots, 4$), and eight *corner* Lagrange multipliers $\lambda_{i,j}$ on $\Gamma_{i,j}$ (with $i, j = 1, \ldots, 4$ such that Γ_i and Γ_j are adjacent). These multipliers will be used to enforce the following continuity conditions:

$$\begin{aligned} u - u_i &= 0 \quad \text{on each } \Gamma_i, \\ u_i - u_{i,j} &= 0 \quad \text{on each } \Gamma_{i,j}. \end{aligned} \tag{5}$$

The dualization of these continuity conditions leads that Lagrange multipliers that weakly verify

$$\begin{aligned} \lambda_i &= \mathbf{n}_i \cdot (\mathbb{D}_i \, \mathbf{grad}\, u_i) \qquad \text{on each } \Gamma_i, \\ \lambda_{i,j} &= \mathbf{n}_{i,j} \cdot (\mathbb{D}_{i,j} \, \mathbf{grad}\, u_{i,j}) \quad \text{on each } \Gamma_{i,j}, \end{aligned} \tag{6}$$

which corresponds to the required Neumann traces that appear in the definition of the subproblems. Let us note that $\lambda_{i,j} \neq \lambda_{j,i}$.

In order to write the variational formulation in a concise form, we introduce the set of u-fields, denoted u_{all}, defined such that the restriction of u_{all} on Ω, Ω_i and $\Omega_{i,j}$ is respectively u, u_i and $u_{i,j}$. Similarly, the set of λ-fields, denoted λ_{all}, is defined such that the restriction of λ_{all} on Γ_i and $\Gamma_{i,j}$ is respectively λ_i and $\lambda_{i,j}$. The sets of fields u_{all} and λ_{all} belong to the following functional spaces:

$$\mathcal{U} := H^1(\Omega) \oplus \left[\bigoplus_i H^1(\Omega_i) \right] \oplus \left[\bigoplus_{i,j} H^1(\Omega_{i,j}) \right], \tag{7}$$

$$\mathcal{L} := \left[\bigoplus_i H^{-1/2}(\Gamma_i) \right] \oplus \left[\bigoplus_{i,j} H^{-1/2}(\Gamma_{i,j}) \right], \tag{8}$$

where $H^{-1/2}(\cdot)$ is the dual space of the Dirichlet trace space $H^{1/2}(\cdot)$. The variational formulation of the problem then reads: Find $(u_{\text{all}}, \lambda_{\text{all}}) \in \mathcal{U} \times \mathcal{L}$ such that

$$\begin{cases} h(u_{\text{all}}, v_{\text{all}}) + \overline{c(\lambda_{\text{all}}, v_{\text{all}})} = l(v_{\text{all}}), \\ c(u_{\text{all}}, \mu_{\text{all}}) = 0, \end{cases} \tag{9}$$

holds for all test functions $(v_{\text{all}}, \mu_{\text{all}}) \in \mathcal{U} \times \mathcal{L}$, where the sesquilinear forms and the antilinear form are defined as

$$\begin{aligned} h(u_{\text{all}}, v_{\text{all}}) := & \int_\Omega - \mathbf{grad}\, u \cdot \mathbf{grad}\, \bar{v} + k^2 u \bar{v} \, \mathrm{d}\Omega \\ & + \sum_i \int_{\Omega_i} -\mathbb{D}_i \, \mathbf{grad}\, u_i \cdot \mathbf{grad}\, \bar{v}_i + E_i k^2 u_i \bar{v}_i \, \mathrm{d}\Omega_i \\ & + \sum_{i,j} \int_{\Omega_{i,j}} -\mathbb{D}_{i,j} \, \mathbf{grad}\, u_{i,j} \cdot \mathbf{grad}\, \bar{v}_{i,j} + E_{i,j} k^2 u_{i,j} \bar{v}_{i,j} \, \mathrm{d}\Omega_{i,j}, \end{aligned} \tag{10}$$

$$c(u_{\text{all}}, \mu_{\text{all}}) := \sum_i \int_{\Gamma_i} (u - u_i) \bar{\mu}_i \, \mathrm{d}\Gamma_i + \sum_{i,j} \int_{\Gamma_{i,j}} (u_i - u_{i,j}) \bar{\mu}_{i,j} \, \mathrm{d}\Gamma_{i,j}, \tag{11}$$

$$l(v_{\text{all}}) := - \int_\Omega f \bar{v} \, \mathrm{d}\Omega. \tag{12}$$

The form $h(\cdot, \cdot)$ is the standard sesquilinear form for the Helmholtz equation with the PML material parameters, and the form $c(\cdot, \cdot)$ corresponds to the coupling with the Lagrange multipliers. The overline $\bar{\cdot}$ denotes the complex conjugate of a field.

2.3. Finite element discretizations

For the finite element discretization of Problem (9), we consider two conformal approximation spaces, $\mathcal{U}^h \subset \mathcal{U}$ and $\mathcal{L}^h \subset \mathcal{L}$, and the discrete fields $u^h_{\text{all}} \in \mathcal{U}^h$ and $\lambda^h_{\text{all}} \in \mathcal{L}^h$. The approximate variational formulation then reads: Find $\left(u^h_{\text{all}}, \lambda^h_{\text{all}}\right) \in \mathcal{U}^h \times \mathcal{L}^h$ such that

$$\begin{cases} h(u^h_{\text{all}}, v^h_{\text{all}}) + \overline{c(\lambda^h_{\text{all}}, v^h_{\text{all}})} = l(v^h_{\text{all}}), \\ c(u^h_{\text{all}}, \mu^h_{\text{all}}) = 0, \end{cases} \tag{13}$$

holds for every test function $\left(v^h_{\text{all}}, \mu^h_{\text{all}}\right) \in \mathcal{U}^h \times \mathcal{L}^h$. This formulation leads to the following linear system:

$$\begin{pmatrix} \mathsf{U} & \mathsf{L}^T \\ \mathsf{L} & 0 \end{pmatrix} \begin{pmatrix} \mathsf{u}^h_{\text{all}} \\ \mathsf{l}^h_{\text{all}} \end{pmatrix} = \begin{pmatrix} \mathsf{f} \\ 0 \end{pmatrix}, \tag{14}$$

where U is a block matrix derived form the sesquilinear form $h(\cdot, \cdot)$, L is a block matrix coming form the sesquilinear form $c(\cdot, \cdot)$ and f is the source vector. The vectors $\mathsf{u}^h_{\text{all}}$ and $\mathsf{l}^h_{\text{all}}$ contain the degrees of freedom associated to the discrete solution and the Lagrange multipliers, respectively. Let us note that U does not depend on the approximation space $\mathcal{L}^h$, while L does.

In this work, the space $\mathcal{U}^h$ is built by using standard hierarchical H^1-conforming basis functions. The approximation space for the Lagrange multipliers, $\mathcal{L}^h$, is based either on hierarchical H^1-conforming basis functions (choice called *"continuous discretization"*) or on the projection of hierarchical $\mathbf{H}(\text{div})$-conforming basis functions on the normal of the each interface (choice called *"discontinuous discretization"*). As we will see, this choice influences the well-posedness of Problem (13): the algebraic system may not be solvable and stability issues may arise. Both discretizations are described and strategies to address these issues are discussed in Sections 2.3.1 and 2.3.2.

We recall herafter the conditions for the well-posedness of Problem (13) (see e.g. [9, 23]).

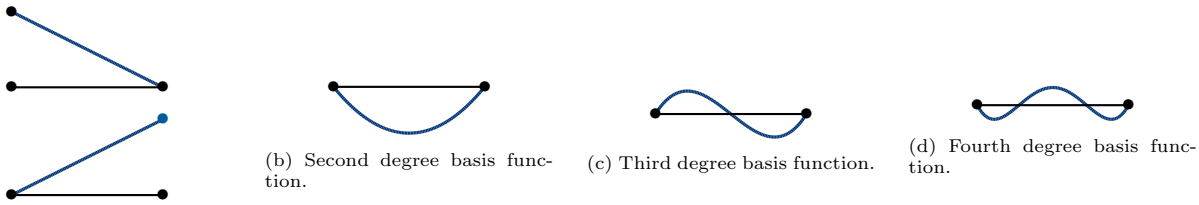

(a) First degree basis functions (classical P1).

(b) Second degree basis function.

(c) Third degree basis function.

(d) Fourth degree basis function.

Figure 2: Hierarchical H^1-conforming basis functions

Theorem 1. (Well-posedness) *Problem (13) is well-posed if and only if there exist positive constants β and γ, independent of the mesh-size h, such that*

$$\inf_{u^h_{all}\in\mathcal{K}} \sup_{v^h_{all}\in\mathcal{K}} \frac{|h(u^h_{all}, v^h_{all})|}{\|u^h_{all}\|_{\mathcal{U}^h}\|u^h_{all}\|_{\mathcal{U}^h}} \geq \beta \tag{15}$$

$$\inf_{\mu^h_{all}\in\mathcal{L}^h} \sup_{u^h_{all}\in\mathcal{U}^h} \frac{|c(u^h_{all}, \mu^h_{all},)|}{\|u^h_{all}\|_{\mathcal{U}^h}\|\mu^h_{all}\|_{\mathcal{L}^h}} \geq \gamma \tag{16}$$

where $\|\cdot\|_{\mathcal{U}^h}$ and $\|\cdot\|_{\mathcal{L}^h}$ are norms associated to the approximation spaces $\mathcal{U}^h$ and $\mathcal{L}^h$, and $\mathcal{K}$ is the kernel of the operator associated to the sesquilinear form $c(\cdot,\cdot)$ in $\mathcal{U}^h$.

This theorem implies the existence and the uniqueness of the solution for any given mesh, and the stability of the problem with stability constants independent of the mesh. The following theorem gives the solvability conditions for System (14).

Theorem 2. (Solvability) *For a given mesh, the matrix of problem (14) is non singular if and only if the following two conditions are both satisfied:*

1. $\mathsf{U}_{KK} : K \to K$ *is surjective (or, equivalently, is injective),*
2. $\mathsf{L} : \mathbb{C}^n \to \mathbb{C}^m$ *is surjective (or, equivalently, L^T is injective),*

where U_{KK} is the projection of U into the kernel K of L.

If the solution belongs to the kernel of L, the second line of System (14) is verified. This line corresponds to relations that are enforced with the Lagrange multipliers. Assuming that the approximate solution is continuous at the interfaces thanks to the Lagrange multipliers, the resulting problem corresponds to the discretization of the standard Helmholtz problem with PML over Ω_{all}, which is well-posed [6–8].

2.3.1. Strategies with continuous Lagrange multipliers

In the first approach, the approximation space $\mathcal{L}^h$ is built by using hierarchical H^1-conforming basis functions on each interface. Then, the Lagrange multipliers are continuous over each interface. We assume that the same polynomial degree is used for both $\mathcal{L}^h$ and $\mathcal{U}^h$. The basis functions used for $\mathcal{L}^h$ then correspond to the restriction on the interfaces of the basis functions used for $\mathcal{U}^h$. The very first basis functions correspond to standard P1 finite elements, and the high-order basis functions are built by using the approach described *e.g.* in [57]. The basis functions for the one-dimensional case are represented on Figure 2.

Unfortunately, the direct implementation of Problem (13) with continuous Lagrange multipliers leads to algebraic systems that are not solvable. Indeed, L is not surjective (or, equivalently, L^T is not injective), and the second solvability condition of Theorem 2 is not met. It can be shown by considering the relations verified on the interfaces around the cross-point $C_{1,2}$, represented on Figure 1c. The continuity of the discrete

solution is enforced weakly by using the following relations:

$$\int_{\Gamma_1} (u^h - u_1^h)\bar{\mu}_1^h \, \mathrm{d}\Gamma_1 = 0, \tag{17}$$

$$\int_{\Gamma_2} (u^h - u_2^h)\bar{\mu}_2^h \, \mathrm{d}\Gamma_2 = 0, \tag{18}$$

$$\int_{\Gamma_{1,2}} (u_1^h - u_{1,2}^h)\bar{\mu}_{1,2}^h \, \mathrm{d}\Gamma_{1,2} = 0, \tag{19}$$

$$\int_{\Gamma_{2,1}} (u_2^h - u_{1,2}^h)\bar{\mu}_{2,1}^h \, \mathrm{d}\Gamma_{2,1} = 0, \tag{20}$$

where the test functions belong to the approximation spaces associated to the Lagrange multipliers. In these relations, the discrete solutions, u^h, u_1^h, u_2^h and $u_{1,2}^h$, can be replaced by their representations with the basis functions. Only the degrees of freedom associated to the interfaces are involved in these relations. The discrete solutions appearing in Equation (17) can be written as

$$u^h|_{\Gamma_1} = \sum_j u^{h,j}\phi_j|_{\Gamma_1} \qquad \text{and} \qquad u_1^h|_{\Gamma_1} = \sum_j u_1^{h,j}\phi_{1,j}|_{\Gamma_1}, \tag{21}$$

where ϕ_j and $\phi_{1,j}$ denote basis functions of u^h and u_1^h associated to the interface Γ_1. The sums are preformed over the J degrees of freedom of u^h associated to Γ_1 and the J_1 degrees of freedom of u_1^h associated to Γ_1. Finally, substituting these expressions into Equation (17), and using the basis functions of the Lagrange multipliers, $\{\psi_{1,i}\}_{i=1,\dots,I}$, as test functions leads to

$$\int_{\Gamma_1} \left(\sum_j u^{h,j}\phi_j - \sum_j u_1^{h,j}\phi_{1,j} \right) \psi_{1,i} \, \mathrm{d}\Gamma_1 = 0 \qquad \text{for } i = 1, \dots, I. \tag{22}$$

Denoting u^h and u_1^h the vectors of degrees of freedom associated to the interface Γ_1, we obtain

$$\mathsf{M}_{\Gamma_1}\mathsf{u}^h - \mathsf{M}_{1,\Gamma_1}\mathsf{u}_1^h = 0, \tag{23}$$

where

$$(\mathsf{M}_{\Gamma_1})_{ij} = \int_{\Gamma_1} \phi_j \, \psi_{1,i} \, \mathrm{d}\Gamma \qquad \text{and} \qquad (\mathsf{M}_{1,\Gamma_1})_{ij} = \int_{\Gamma_1} \phi_{1,j} \, \psi_{1,i} \, \mathrm{d}\Gamma \tag{24}$$

are mass matrices of size $I \times J$ and $I \times J_1$, respectively. If the same polynomial degree is used for the finite element approximation of the fields u^h, u_1^h and μ_1^h, the corresponding basis functions are identical on the interface Γ_1. Then, Equation (23) can be rewritten as

$$\mathsf{M}_{\Gamma_1}^{\text{cont}} \left(\mathsf{u}^h - \mathsf{u}_1^h \right) = 0, \tag{25}$$

and $\mathsf{M}_{\Gamma_1}^{\text{cont}}$ is a standard square mass matrix. Since this matrix is non-singular, we have $\mathsf{u}^h = \mathsf{u}_1^h$, and then $u^h|_{\Gamma_1} = u_1^h|_{\Gamma_1}$. In particular, the degrees of freedom of u^h and u_1^h associated to the cross-point $C_{1,2}$ are equal, *i.e.* $u^C = u_1^C$. The basis functions associated to the cross-point $C_{1,2}$ are represented on Figure 3. The same reasoning can be carried out for the other interfaces around the cross-point $C_{1,2}$, leading to the following relations,

$$u^C = u_1^C, \tag{26}$$

$$u^C = u_2^C, \tag{27}$$

$$u_1^C = u_{1,2}^C, \tag{28}$$

$$u_2^C = u_{1,2}^C, \tag{29}$$

where u_2^C and $u_{1,2}^C$ are the degrees of freedom at the cross-point associated to u_2^h and $u_{1,2}^h$. Because these relations are linear dependent, there is also a linear dependency between the relations resulting from the discretization of (17)-(20). Therefore, L is not surjective, and Problem (14) is not solvable.

Several approaches can be used to recover the surjectivity of matrix L, and then to make Problem (14) solvable:

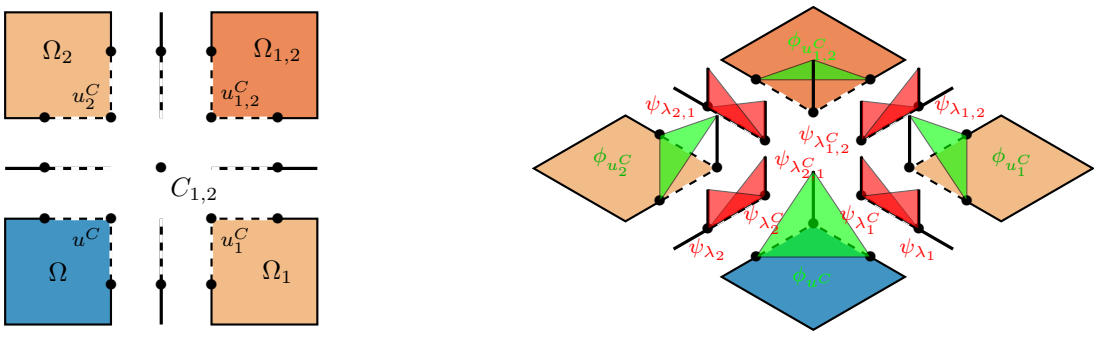

Figure 3: Degrees of freedom and P1 basis functions involved around the cross-point $C_{1,2}$

1. An additional constraint on the unknowns can be added in order to avoid the linear dependency between Equations (26)-(29). This can be done by introducing an additional Lagrange multiplier, denoted λ^C, associated to the cross-point. In this work, the following constraint is used:

$$\lambda_1^C - \lambda_2^C + \lambda_{1,2}^C - \lambda_{2,1}^C = 0, \quad \text{at } C_{1,2}, \tag{30}$$

   where λ_1^C, λ_2^C, $\lambda_{1,2}^C$ and $\lambda_{2,1}^C$ are the Lagrange multipliers associated to the interfaces around the cross-point $C_{1,2}$. Then, terms involving λ^C are introduced in the relations associated to these multipliers, in such a way that Equations (26)-(29) become

$$u^C = u_1^C + \lambda^C, \tag{31}$$
$$u^C = u_2^C - \lambda^C, \tag{32}$$
$$u_1^C = u_{1,2}^C + \lambda^C, \tag{33}$$
$$u_2^C = u_{1,2}^C - \lambda^C. \tag{34}$$

   These relations are not longer linearly dependent, and Problem (14) with the supplementary equation becomes solvable. A similar strategy was used by Peng and Lee [53] to improve a domain decomposition method for time-harmonic electromagnetic problems.
2. A penalization strategy (see *e.g.* [9]), where a mass matrix is added in Problem (14), can be used to obtain the following modified system:

$$\begin{pmatrix} \mathsf{U} & \mathsf{L}^T \\ \mathsf{L} & \tau\mathsf{M} \end{pmatrix} \begin{pmatrix} \mathsf{u}_{\text{all}}^h \\ \mathsf{l}_{\text{all}}^h \end{pmatrix} = \begin{pmatrix} \mathsf{f} \\ 0 \end{pmatrix}, \tag{35}$$

   where τ is a penalization parameter to be tuned and M is the standard mass matrix associated to the Lagrange multiplier space $\mathcal{L}^h$. Because of the new block, the continuity conditions (5) are not exactly verified. They become

$$\begin{aligned} u - u_i &= \tau\lambda_i, \quad \text{on each } \Gamma_i, \\ u_i - u_{i,j} &= \tau\lambda_{i,j}, \quad \text{on each } \Gamma_{i,j}. \end{aligned} \tag{36}$$

   Thanks to the penality, a right-hand-side term is added to Equation (25), and the linear dependency between the relations at the corner is avoided.
3. A last strategy consists in taking approximate fields with different polynomial degrees in the domain and the PML regions. In preliminary tests (not shown), we have observed that, if the polynomial degree in the edge PMLs and the corner PMLs is larger by one and two, respectively, than in the domain, then the system is solvable. This strategy, which involves much more degrees of freedom than the others, will not be investigated further in this work.

Let us highlight that continuity of the Dirichlet traces at the interfaces is preserved exactly with the first strategy, but it is relaxed with the two last ones.

(a) First degree basis function.

(b) Second degree basis function.

(c) Third degree basis function.

(d) Fourth degree basis function.

Figure 4: Hierarchical $\mathbf{H}(\mathrm{div})$-conforming basis functions

2.3.2. Strategies with discontinuous Lagrange multipliers

For the second approach, the basis functions of the approximation space $\mathcal{L}^h$ correspond to the projection of hierarchical $\mathbf{H}(\mathrm{div})$-conforming basis functions (defined on the domain and the PML regions) on the normal to the interfaces. In two dimensions, the hierarchical $\mathbf{H}(\mathrm{div})$-conforming basis functions correspond to the 90-degree rotation of $\mathbf{H}(\mathbf{curl})$-conforming basis functions. The first-order $\mathbf{H}(\mathbf{curl})$-conforming basis functions are the Nédélec basis functions [49, 50], and the higher-order functions are associated to the edges and the face of the elements (see *e.g.* [57]). The first basis functions for the Lagrange multipliers are represented on Figure 4. By contrast with the previous discretization, the basis functions are discontinuous between the elements, and the continuity of the Lagrange multipliers is not ensured. This approach is called the *discontinuous discretization*.

Depending on the polynomial degree used for the discontinuous Lagrange multipliers, the solvability issue discussed in the previous section can be naturally avoided. Indeed, with the discontinuous discretization, System (22) can be rewritten as

$$\mathsf{M}_{\Gamma_1}^{\mathrm{disc}} \left(\mathsf{u}^h - \mathsf{u}_1^h \right) = 0, \tag{37}$$

where $\mathsf{M}_{\Gamma_1}^{\mathrm{disc}}$ is a rectangular mass matrix associated to the discontinuous basis functions $\{\psi_{1,i}\}_i$ used for the Lagrange multipliers and the continuous basis functions $\{\phi_j\}_j$ used for the discrete solutions (see Equation (24)). This matrix cannot be square. If the polynomial degree of the Lagrange multipliers is lower than or equal to the degree of the discrete solution, then the system is underdetermined and $\mathsf{u}^h = \mathsf{u}_1^h$ does not hold. In this case, the continuity of the discrete solution at the interfaces is not exactly verified, but the system is solvable since L is full-rank. In the opposite case, Equation (37) is a homogeneous overdetermined system, and $\mathsf{u}^h = \mathsf{u}_1^h$ is the trivial solution. The problem in not solvable because L is not surjective, but the penalization strategy developed in the previous section can be used to make it solvable.

Unfortunately, we have observed that the problem is not stable if the same polynomial degree is used for both the discontinuous Lagrange multipliers and the discrete solutions. In that case, the first inf-sup condition of Theorem 1 is *a priori* not met, and the problem is not well-posed. For many practical situations, it is difficult to prove the first inf-sup condition. This is why, a numerical Chapelle-Bath test [2, 3] is applied to evaluate the inf-sup constant β for the different discretizations. In a nutshell, a modified version of the system is considered,

$$\begin{pmatrix} \mathsf{U} & \mathsf{L}^T \\ \mathsf{L} & -\frac{1}{s}\mathsf{M} \end{pmatrix} \begin{pmatrix} \mathsf{u}_{\mathrm{all}}^h \\ \mathsf{l}_{\mathrm{all}}^h \end{pmatrix} = \begin{pmatrix} \mathsf{f} \\ 0 \end{pmatrix}, \tag{38}$$

where s is a positive constant and M is the mass matrix associated to the Lagrange multipliers. Taking $s \to \infty$ brings back the original system (14). The inf–sup test consists in checking that, using a sequence of meshes with decreasing mesh size h, the first non-vanishing eigenvalue α_h of the problem

$$\frac{1}{h}(\mathsf{L}^T\mathsf{M}^{-1}\mathsf{L})\mathsf{v}_h = \alpha_h \mathsf{U}^T\mathsf{v}_h, \tag{39}$$

does not depend too much on the mesh size h. Further, the inf-sup constant is given by $\beta = \min_h \beta_h$, with $\beta_h := \alpha_h^2$.

In Figure 5a, the value β_h is plotted for the continuous and the discontinuous discretizations of the Lagrange multipliers with several stabilization strategies. These results are obtained for a benchmark with the square domain $[-1,1]\times[-1,1]$, meshes with cell sizes from $h = 0.03$ to 0.32, the polynomial degree $p = 2$ for the discrete solution, and the penalization parameter $\tau = 0.002\ h^2$. When the discontinuous discretization

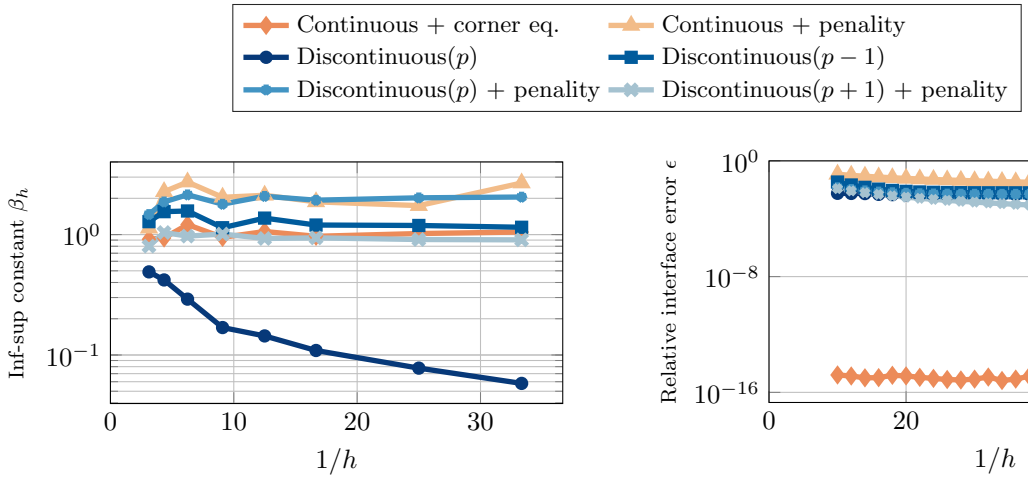

(a) Numerical evaluation of the inf-sup constant of Theorem 1 obtained for u-field discretized at polynomial degree $p = 2$.

(b) The relative interface error shows that discontinuous discretizations (stabilized or not) introduce a lack of continuity at interfaces compared to the continuous discretization.

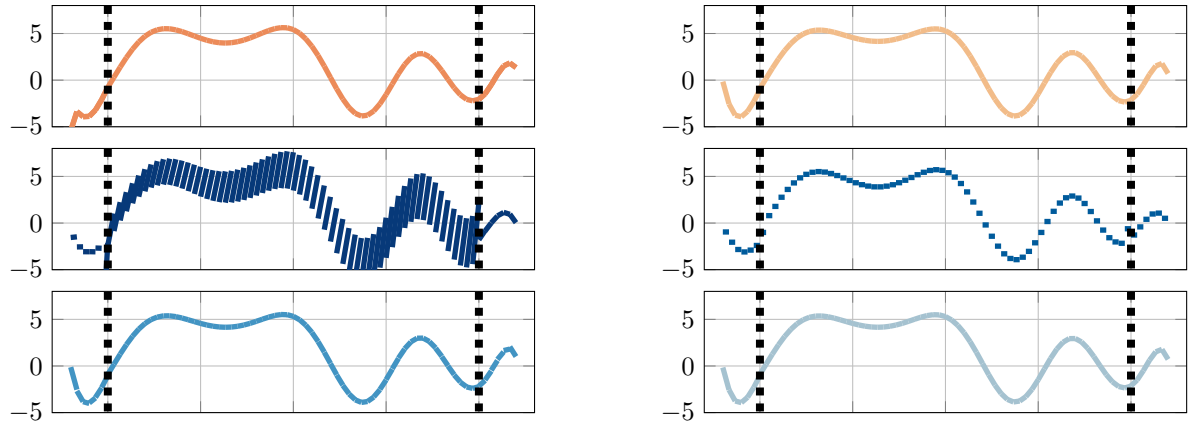

(c) Neumann traces along interface $\Gamma_{3,2} \cup \Gamma_2 \cup \Gamma_{1,2}$ (u-field discretized at polynomial degree $p = 2$).

Figure 5: Interface issues and Neumann traces.

is used with the same polynomial degree for both the Lagrange multipliers and the discrete solution, the value β_h decreases significantly with $1/h$, which indicates that the formulation is not stable, as mentionned earlier. By contrast, we observe that the other combinations are stable.

To study the effect of the discretization of the Lagrange multipliers on the discrete solution, we consider the relative continuity error at the interfaces, defined as

$$\epsilon = \frac{\sum_i \int_{\Gamma_i} \|u - u_i\|^2 \, \mathrm{d}\Gamma_i + \sum_{i,j} \int_{\Gamma_{i,j}} \|u_i - u_{i,j}\|^2 \, \mathrm{d}\Gamma_{i,j}}{\sum_i \int_{\Gamma_i} \|u\|^2 \, \mathrm{d}\Gamma_i + \sum_{i,j} \int_{\Gamma_{i,j}} \|u_i\|^2 \, \mathrm{d}\Gamma_{i,j}}. \tag{40}$$

This error is plotted according to the mesh size on Figure 5b for the different approaches. As expected, only the continuous discretization with the cross-point treatment leads to the perfect continuity of the Dirichlet trace (*i.e.* the relative error ϵ is close to the machine epsilon). Only that approach enforces exactly the continuity of the discrete field, while the continuity is relaxed with the other ones. The Neumann trace computed on the upper interface of Figure 1, namely on $\Gamma_{3,2} \cup \Gamma_2 \cup \Gamma_{1,2}$, is shown on Figure 5c for the different approaches. The trace obtained with the unstable discontinuous discretization clearly oscillates, while the others are smooth.

3. DDM with PML transmission conditions for checkerboard domain partitions

In this section, we present a non-overlapping domain decomposition method (DDM) with PML transmission conditions for checkerboard (Cartesian) domain partitions. Transmission operators based on PMLs have been used to accelerate domain decomposition solvers [58, 64] and preconditioning techniques [1, 41, 56, 62]. However, for domain decomposition solvers with checkerboard domain partitions, an unappropriate treatment of the interior cross-points (*i.e.* points where more than two subdomains meet) and the boundary cross-points (*i.e.* points where an interface meet an exterior border) may lead to suboptimal convergence or even incorrect results. In this work, the PML is used as a DtN operator thanks to the strategies developed in the previous section, leading to a domain decomposition method that naturally takes into account cross-points. The standard non-overlapping DDM is presented in Section 3.1. Modifications to use PMLs as transmission operators and to address cross-points are explained in Sections 3.2 and 3.3.

3.1. Non-overlapping domain decomposition algorithm

To describe the standard DDM, we consider a simple Helmholtz problem defined on a rectangular domain, denoted Ω_{glo},

$$\begin{cases} \Delta\, u + k^2 u = -f, & \text{in } \Omega_{\text{glo}}, \\ \partial_{\mathbf{n}} u + \mathcal{B} u = 0, & \text{on } \partial\Omega_{\text{glo}}, \end{cases} \tag{41}$$

where k is the (positive) wavenumber, f is a source term, $\partial_{\mathbf{n}}$ is the outgoing normal derivative on the boundary $\partial\Omega_{\text{glo}}$, and $\mathcal{B}$ is a boundary operator. The domain will be surrounded with PMLs to simulate outgoing waves, and the operator $\mathcal{B}$ will be defined accordingly by using techniques described in the previous section.

The global domain Ω_{glo} is decomposed into N non-overlapping rectangular subdomains Ω_n, with $n = 1, \dots, N$, on a two-dimensional grid (see illustration on Figure 6a for $N = 4$). The edges of each subdomain Ω_n are denoted $\Sigma_{n,i}$, with $i = 1, \dots, 4$. An edge can be either a *boundary edge* if it belongs to the boundary of Ω_{glo} (*i.e.* $\Sigma_{n,i} \subset \partial\Omega_{\text{glo}}$), or an *interface edge* if it is shared by two subdomains (*i.e.* $\Sigma_{n,i} \not\subset \partial\Omega_{\text{glo}}$). For each subdomain Ω_n, we consider the local solution u_n of the subproblem

$$\begin{cases} \Delta\, u_n + k^2 u_n = -f, & \text{in } \Omega_n, \\ \partial_{\mathbf{n}_{n,i}} u_n + \mathcal{T}_{n,i} u_n = g_{n,i}, & \text{on each } \Sigma_{n,i}, \end{cases} \tag{42}$$

where $\mathcal{T}_{n,i}$ is a transmission operator and $g_{n,i}$ is a transmission variable defined as

$$g_{n,i} := \begin{cases} 0 & \text{if } \Sigma_{n,i} \subset \partial\Omega_{\text{glo}}, \\ \partial_{\mathbf{n}_{n,i}} u_m + \mathcal{T}_{n,i} u_m & \text{if } \Sigma_{n,i} \not\subset \partial\Omega_{\text{glo}}, \end{cases} \tag{43}$$

where u_m is the local solution on Ω_m, that is the neighboring subdomain of Ω_n sharing the interface edge. If $\Sigma_{n,i}$ is a boundary edge, the transmission operator $\mathcal{T}_{n,i}$ is simply a boundary operator. The variational formulation of the subproblem reads: Find $u_n \in H^1(\Omega_n)$ such that

$$\begin{aligned} \int_{\Omega_n} -\mathbf{grad}\, u_n \cdot \mathbf{grad}\, \bar{v}_n + k^2 u_n \bar{v}_n \, \mathrm{d}\Omega_n - \sum_i \int_{\Sigma_{n,i}} (\mathcal{T}_{n,i} u_n) \bar{v}_n \, \mathrm{d}\Sigma_{n,i} \\ = -\int_{\Omega_n} f \bar{v}_n \, \mathrm{d}\Omega_n - \sum_i \int_{\Sigma_{n,i}} g_{n,i} \bar{v}_n \, \mathrm{d}\Sigma_{n,i}, \end{aligned} \tag{44}$$

holds for all test function $v_n \in H^1(\Omega_n)$.

At every step of an iterative procedure, a subproblem similar to Problem (44) is solved for every subdomain Ω_n. Then, the transmission variables are updated and exchanged between the subdomains. Since System (42) is defined for every subdomain, the transmission condition

$$\partial_{\mathbf{n}_{m,i'}} u_m + \mathcal{T}_{m,i'} u_m = g_{m,i'}, \tag{45}$$

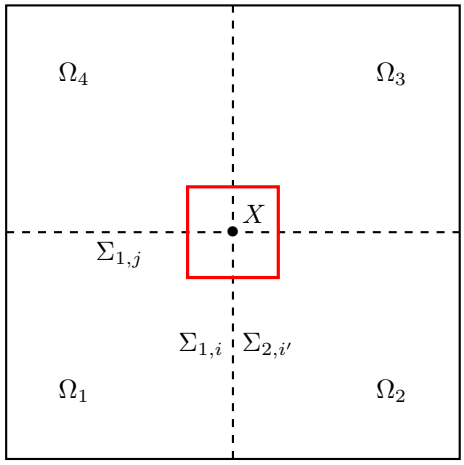

(a) Decomposition of a square domain Ω_{glo} into four subdomains Ω_n leading to a cross-point X at the intersection between the four subdomains.

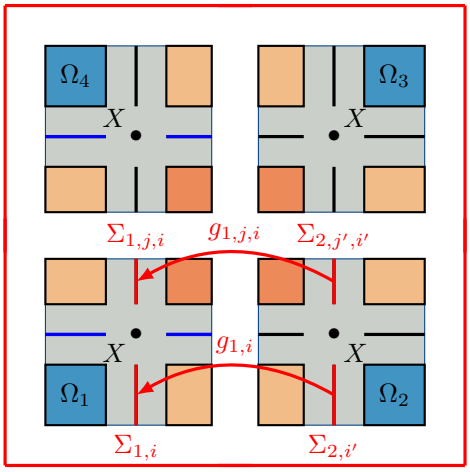

(b) Zoom on the cross-point of Figure 6a (the red box) to see how data are exchanged in the case of a PML-based DDM. (For clarity the unique cross-point X is drawn four times and the domains are represented with a shift.)

Figure 6: Four subdomains and a cross-point X between them.

is prescribed on the interface edge $\Sigma_{m,i'}$ of Ω_m, where i' is such that $\Sigma_{n,i} = \Sigma_{m,i'}$. Assuming that the transmission operator is symmetric (*i.e.* $\mathcal{T}_{n,i} = \mathcal{T}_{m,i'}$), Equations (43) and (45) give

$$g_{n,i} = -g_{m,i'} + 2\mathcal{T}_{m,i'} u_m. \tag{46}$$

This relation is used to define the update formula for the transmission variables,

$$g_{n,i}^{(\ell+1)} = -g_{m,i'}^{(\ell)} + 2\mathcal{T}_{m,i'} u_m^{(\ell)}. \tag{47}$$

where ℓ is the index of the iterative procedure. The update of all the transmission variables can be rewritten as a fixed-point algorithm applied to a global transmission problem (see *e.g.* [61]). In practice, this global problem can be solved by using Krylov subspace methods. In this work, GMRES is used.

3.2. The PML-based transmission operator

The PML can be used rather naturally as a DtN operator thanks to the weak coupling introduced in the previous section. With that approach, the continuity of the solution at the interface between the PML and a given domain is enforced weakly thanks to a Lagrange multiplier, and the value of this multiplier can be interpreted as the Neumann trace of the solution. Therefore, the PML can be seen as an operator taking a Dirichlet trace and returning the corresponding Neumann trace. For the interface edge $\Sigma_{n,i}$ of subdomain Ω_n, the transmission operator $\mathcal{T}_{n,i}$ is formally defined as

$$\mathcal{T}_{n,i} \ : \ H^{1/2}(\Sigma_{n,i}) \ \mapsto \ H^{-1/2}(\Sigma_{n,i}) \ : \ u_n|_{\Sigma_{n,i}} \ \mapsto \ \mathcal{T}_{n,i} u_n := \lambda_{n,i}, \quad (= \partial_{\mathbf{n}_{n,i}} u_n|_{\Sigma_{n,i}}) \tag{48}$$

where $\lambda_{n,i}$ is the Lagrange multiplier used to prescribed the continuity of the solution at the interface between the subdomain and the PML.

In order to clarify the use of the PML-based DtN operator in the DDM, let us consider a rectangular waveguide partitionned into successive layers, with a homogeneous Neumann boundary condition on the lateral borders. In this configuration, every subdomain Ω_n has two neighbors, expect both subdomains that are at the extremities of the partition. At both interface edges, denoted $\Sigma_{n,1}$ and $\Sigma_{n,2}$, the subdomain is extended with two PMLs, denoted $\Omega_{n,1}$ and $\Omega_{n,2}$, respectively. The variational formulation (44) associated to Ω_n can be written as: Find $(u_n, u_{n,1}, u_{n,2}) \in H^1(\Omega_n) \times H^1(\Omega_{n,1}) \times H^1(\Omega_{n,2})$ and $(\lambda_{n,1}, \lambda_{n,2}) \in H^{-1/2}(\Sigma_{n,1}) \times$

$H^{-1/2}(\Sigma_{n,2})$ such that

$$\int_{\Omega_n} \big(-\mathbf{grad}\, u_n \cdot \mathbf{grad}\, \bar{v}_n + k^2 u_n \bar{v}_n \big)\, \mathsf{d}\Omega_n + \sum_i \int_{\Omega_{n,i}} \big(-\mathbb{D}_{n,i}\, \mathbf{grad}\, u_{n,i} \cdot \mathbf{grad}\, \bar{v}_{n,i} + E_{n,i}\, k^2 u_{n,i} \bar{v}_{n,i} \big)\, \mathsf{d}\Omega_{n,i} + \sum_i \int_{\Sigma_{n,i}} \lambda_{n,i} (\bar{v}_n - \bar{v}_{n,i})\, \mathsf{d}\Sigma_{n,i} = -\int_{\Omega_n} f \bar{v}_n\, \mathsf{d}\Omega_n - \sum_i \int_{\Sigma_{n,i}} g_{n,i} \bar{v}_n\, \mathsf{d}\Sigma_{n,i}, \quad (49)$$

holds for all test functions $(v_n, v_{n,1}, v_{n,2}) \in H^1(\Omega_n) \times H^1(\Omega_{n,1}) \times H^1(\Omega_{n,2})$, and

$$\sum_i \int_{\Sigma_{n,i}} (u_n - u_{n,i}) \bar{\mu}_{n,i}\, \mathsf{d}\Sigma_{n,i} = 0 \quad (50)$$

holds for all test functions $(\mu_{n,1}, \mu_{n,2}) \in H^{-1/2}(\Sigma_{n,1}) \times H^{-1/2}(\Sigma_{n,2})$. The transmission variables are updated using the Lagrange multipliers. The update formula (47) becomes

$$g_{n,i}^{(\ell+1)} = -g_{m,i'}^{(\ell)} + 2\lambda_{m,i'}^{(\ell)}. \quad (51)$$

To summarize, every subdomain is extended with PMLs (second term in Equation (49)) and Lagrange multipliers are used as Neumann traces in the subdomain (third term in Equation (49)) and the update formula (Equation (51)).

3.3. DDM with PML transmission conditions and cross-point treatment

The approach can be applied to the Helmholtz problem (41) with a checkerboard domain partition. If there is only one subdomain (*i.e.* $N = 1$), the variational formulation (44) should correspond to the original problem with PMLs at the boundaries, leading to the variational formulation (9). If there are more than one subdomain, the same variational formulation can be used for every subdomain, but terms with transmission variables must be added in the right-hand side of the first equation in order to enforce the coupling between the subproblems.

To write the subproblem associated to subdomain Ω_n, we introduce the sets of u_n-fields and λ_n-fields, denoted $u_{n,\mathrm{all}}$ and $\lambda_{n,\mathrm{all}}$, which contain the solutions and the Lagrange multipliers associated to the domain Ω_n, the surrounding PML regions and the interfaces. The corresponding functional spaces are denoted $\mathcal{U}_n$ and $\mathcal{L}_n$. More precise definitions of these objects are provied in Section 2.2 for the problem associated to Ω. The discretization strategies discussed in Section 2.3 will be used.

In the general case, the subproblem associated to Ω_n reads: Find $(u_{n,\mathrm{all}}, \lambda_{n,\mathrm{all}}) \in \mathcal{U}_n \times \mathcal{L}_n$ such that

$$\begin{cases} h_n(u_{n,\mathrm{all}}, v_{n,\mathrm{all}}) + \overline{c_n(\lambda_{n,\mathrm{all}}, v_{n,\mathrm{all}})} = l_n(v_{n,\mathrm{all}}), \\ c_n(u_{n,\mathrm{all}}, \mu_{n,\mathrm{all}}) = 0, \end{cases} \quad (52)$$

where the sesquilinear forms $h_n(\cdot,\cdot)$ and $c_n(\cdot,\cdot)$ are defined similarly to $h(\cdot,\cdot)$ and $c(\cdot,\cdot)$ (see Equations (10) and (11)), and the antilinear form $l_n(\cdot)$ is defined as

$$l_n(v_{n,\mathrm{all}}) := -\int_{\Omega_n} f \bar{v}_n\, \mathsf{d}\Omega_n - \sum_i \int_{\Sigma_{n,i}} g_{n,i} \bar{v}_n\, \mathsf{d}\Sigma_{n,i} - \sum_{i,j} \int_{\Sigma_{n,i,j}} g_{n,i,j} \bar{v}_{n,i}\, \mathsf{d}\Sigma_{n,i,j}. \quad (53)$$

The second term in the right-hand side member of the previous equation introduces a coupling at the interface subdomain-PML for subproblems corresponding to neighboring subdomains. The last term corresponds to a coupling at interfaces PML-PML. These couplings are illustrated on Figure 6b. Let us not that these terms appear only if $\Sigma_{n,i}$ is an interface edge of the subdomain. In that case, the transmission variables are updated using the update relations

$$g_{n,i}^{(\ell+1)} = -g_{m,i'}^{(\ell)} + 2\lambda_{m,i'}^{(\ell)} \qquad \text{on } \Sigma_{n,i} \quad (54)$$

$$g_{n,i,j}^{(\ell+1)} = -g_{m,i',j'}^{(\ell)} + 2\lambda_{m,i',j'}^{(\ell)} \quad \text{on } \Sigma_{n,i,j}, \quad (55)$$

where the variables $g_{n,i}$ and $g_{n,i,j}$ can be considered as *edge* and *corner* transmission variables, respectively, and the Lagrange multipliers $\lambda_{m,i'}$ and $\lambda_{m,i',j'}$ are computed in the subproblem associated to the neighboring subdomain Ω_m. The overscript ℓ corresponds to quantities computed at step ℓ of the iterative procedure. This version of the DDM naturally takes into account cross-points through the definition of the corner transmission variables.

In what follows, the subproblems are solved by using the finite element schemes described in the Section 2. The same discretizations are used for both the Lagrange multipliers and the transmission variables.

4. Numerical results

The performance of the proposed DDM and the discretization strategies for the Lagrange multipliers and the transmission variables are studied by using a reference two-dimensional benchmark described in Section 4.1. First, the continuous and discontinuous discretizations and the different stabilization techniques are compared in Section 4.2, and two approaches are selected. For the selected approaches, the parameters of the PML transmission conditions, namely the absorbing function and the layer thickness, are discussed in Sections 4.3 and 4.4, respectively. The influence of the wavenumber and the mesh density on the convergence of the DDM is analyzed in Section 4.5. Finally, the method is tested with a smoothly varying heterogeneous medium in Section 4.6.

4.1. Description of the reference benchmark and PML parameters

The acoustic scattering of an incident plane wave $u_{\text{inc}}(x) = e^{ikx}$ by a sound-soft disk of radius R is used as reference benchmark. The analytic expression of the scattered field in the polar coordinates (r, θ) for a disk centered at the origin is

$$u_{\text{ref}}(r,\theta) = -\sum_{m=0}^{\infty} \epsilon_m i^m \frac{J_m(kR)}{H_m^{(1)}(kR)} H_m^{(1)}(kr)\cos(m\theta), \quad r > R, \tag{56}$$

where J_m is the m^{th}-order Bessel function, $H_m^{(1)}$ is the m^{th}-order first-kind Hankel function, ϵ_m is a function equal to 1 if $m = 0$ and 2 otherwise, and $i^2 = -1$.

The simulations are performed with a square computational domain, $\Omega_{\text{glo}} = [L_{-x}, L_x] \times [L_{-y}, L_y]$, surrounded with PMLs of thickness δ_{PML}. The material parameters $\mathbb{D}$ and E are defined as

$$\mathbb{D}(x,y) = \text{diag}\left(\frac{\gamma_y(y)}{\gamma_x(x)}, \frac{\gamma_x(x)}{\gamma_y(y)}, \gamma_x(x)\gamma_y(y)\right) \qquad \text{and} \qquad E(x,y) = \gamma_x(x)\gamma_y(y), \tag{57}$$

where $\gamma_x(x)$ and $\gamma_y(y)$ are stretching functions, defined as

$$\gamma_x(x) = 1 + \frac{\sigma_x(x)}{ik} \qquad \text{and} \qquad \gamma_y(y) = 1 + \frac{\sigma_y(y)}{ik}, \tag{58}$$

which depend on absorption functions $\sigma_x(x)$ and $\sigma_y(y)$ associated to the Cartesian directions (see *e.g.* [7, 8]). The functions $\sigma_x(x)$ and $\sigma_y(y)$ are set to zero inside the domain, and they increase along the associated Cartesian directions inside the PMLs. Shifted hyperbolic absorbing functions are used inside the PMLs. Then, the function $\sigma_x(x)$ is defined as

$$\sigma_x(x) = \begin{cases} 1/(\delta_{\text{PML}} - (L_{-x} - x)) - 1/\delta_{\text{PML}} & \text{if } x \in [L_{-x} - \delta_{\text{PML}}, L_{-x}], \\ 1 & \text{if } x \in [L_{-x}, L_x], \\ 1/(\delta_{\text{PML}} - (x - L_x)) - 1/\delta_{\text{PML}} & \text{if } x \in [L_x, L_x + \delta_{\text{PML}}]. \end{cases} \tag{59}$$

The definition is similar for $\sigma_y(y)$. These functions form a couple such that a PML extruded in the x-direction (*i.e.* Ω_1 and Ω_3 on Figure 1a) is associated to $(\sigma_x(x), 0)$, a PML extruded in the y-direction (*i.e.* Ω_2 and Ω_4) is associated to $(0, \sigma_y(y))$, and corner PMLs are associated to $(\sigma_x(x), \sigma_y(y))$.

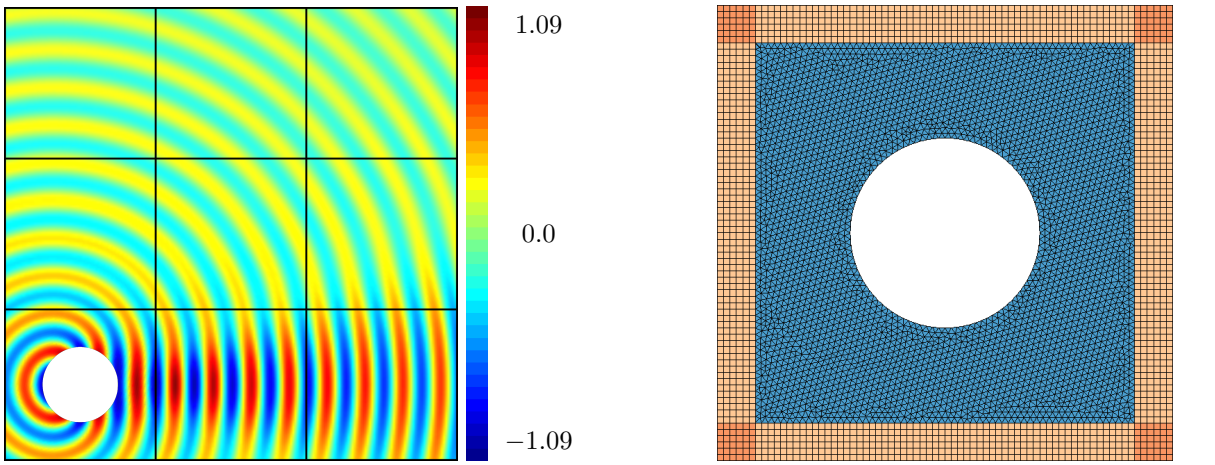

(a) Numerical solution and domain partition

(b) Mesh of one subdomain with the surrounding PMLs

Figure 7: Reference benchmark: scattering of a plane wave by a disk in a square domain with a 3×3 domain partition

For the PML transmission conditions, the material parameters are defined similarly. Let us note that the absorbing functions and the layer thicknesses can be different for the interface edges (*i.e.* in the transmission conditions) and the boundary edges (*i.e.* for the exterior boundary condition) of the domain partition. Different combinations are tested in Sections 4.3 and 4.4.

In the following sections, the DDM is tested with a checkerboard partition of Ω_{glo} into a 3×3 grid with nine square subdomains (see Figure 7a). The disk of radius $R = 0.5$ is placed in the middle of the lower left subdomain, and the borders of the square subdomains are of length 2. Every subdomain is meshed with triangular elements having straight edges, and the surrounding PMLs are generated with extruded square elements, as shown in Figure 7b. The wavenumber is $k = 4\pi$ and the characteristic mesh size is $h \approx 4\pi/15$. The numerical results are obtained with GmshDDM[1], a dedicated `C++` code based on the open-source finite element solver GmshFEM [55], the efficient finite element library based on Gmsh [34].

4.2. Comparison of the discretization strategies for the Lagrange multipliers and the transmission variables

The convergence histories for both continuous and discontinuous discretizations and the different stabilization strategies are presented in Figure 8. For each case, the relative GMRES residual is plotted as a function of the number of GMRES iterations (on the left). The relative L_2-error between the numerical solution and a reference numerical solution is also shown (on the right). This error is computed by comparing the DDM solution u_n in each subdomain with the reference numerical solution u_{mono} computed on Ω_{glo} with the same mesh without domain decomposition procedure,

$$\text{error} = \sqrt{\frac{\sum_{n=1}^{N} \int_{\Omega_n} |u_n - u_{\text{mono}}|^2 \, \mathrm{d}\Omega_n}{\int_{\Omega_{\text{glo}}} |u_{\text{mono}}|^2 \, \mathrm{d}\Omega_{\text{glo}}}}. \tag{60}$$

The u-fields are discretized with hierarchical H^1-conforming basis functions of polynomial degree p equal to 2 and 4. For both boundary and transmission conditions, the PML thickness corresponds to $N_{\text{PML}} = 6$ mesh cells (*i.e.* $\delta_{\text{PML}} = 6h$) and shifted hyperbolic absorbing functions are used.

Let us note that the reference numerical solution u_{mono} is not exactly the same in all the cases. Then, the comparison is not carried out with the same reference problem. Indeed, because the discretization of the Lagrange multipliers is the same for both the exterior boundary condition and the transmission conditions, the reference problem depends on the considered discretization. This approach is chosen because in practice, when a discretization is chosen, it will be used everywhere.

[1]DDM code based on GmshFEM: https://gitlab.onelab.info/gmsh/ddm

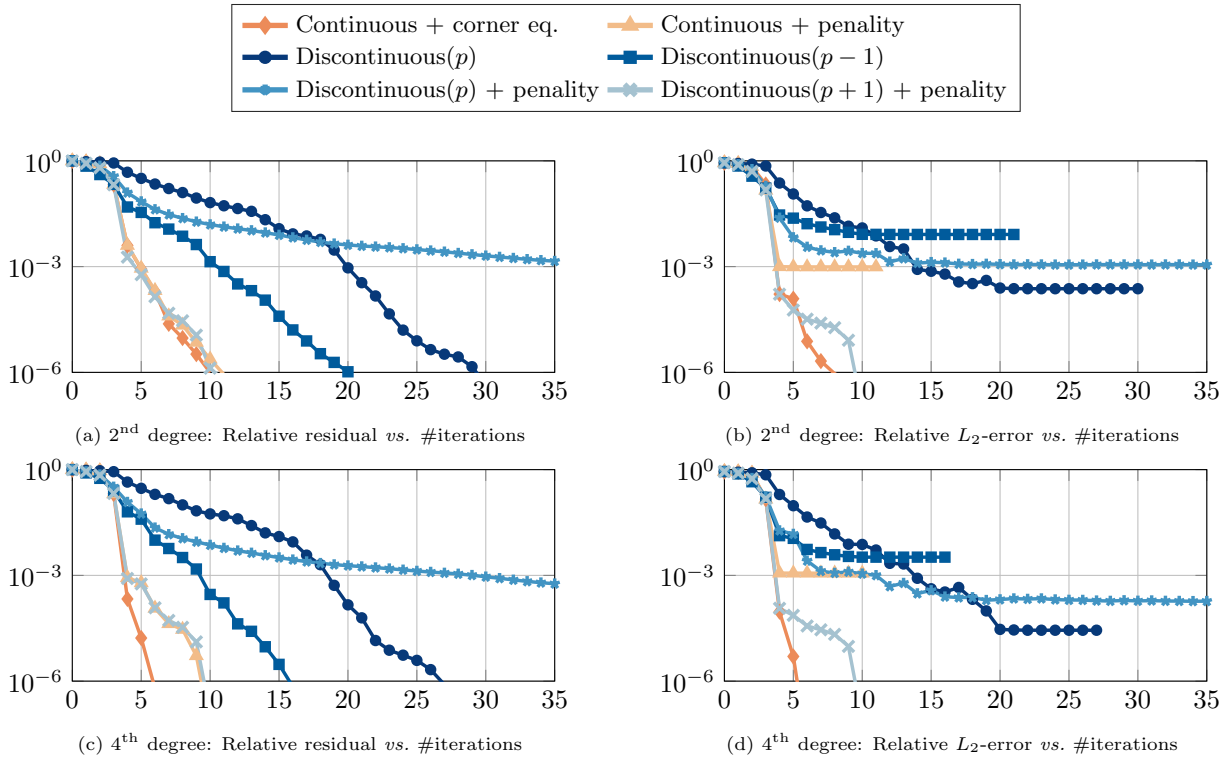

(a) 2^{nd} degree: Relative residual *vs.* #iterations

(b) 2^{nd} degree: Relative L_2-error *vs.* #iterations

(c) 4^{th} degree: Relative residual *vs.* #iterations

(d) 4^{th} degree: Relative L_2-error *vs.* #iterations

Figure 8: Convergence of the relative residual and the relative error for each discretization and stabilization strategy. The computations are performed for $N_{\text{PML}} = 6$, and polynomial degrees $p = 2$ and 4.

	$p = 2$	$p = 4$
Continuous + corner eq.	60	160
Continuous + penality	60	160
Discontinuous(p)	56	154
Discontinuous($p - 1$)	26	100
Discontinuous(p) + penality	56	154
Discontinuous($p + 1$) + penality	98	220

Table 1: The number of degrees of freedom by element thickness for each strategy. The computations are performed for $N_{\text{PML}} = 6$, and polynomial degrees $p = 2$ and 4.

For $p = 2$, the best convergence rate is provided by the continuous discretization (both versions) and the discontinuous discretization with both the polynomial degree $p+1$ and the penalty term (Figure 8a). The decay of residual is slower with the other approaches based on the discontinuous discretization. However, in nearly all the cases, the relative error decreases until a plateau, which the level depends on the case (Figure 8b). This behavior can be explained because, if the discontinuous discretization and/or the penalty strategy is used, the equivalence between the reference problem and the coupled subproblems is not exactly ensured, which introduces an error. The discontinuous discretization with both the higher polynomial degree and the penalty is the notable exception. Similar results are obtained with $p = 4$, except that both the relative residual and the relative error reach 10^{-6} more rapidly with the continuous discretization and the additional corner equation than with all the other approaches.

In order to quantify the relative cost of each strategy, we report in Table 1 the number of degrees of freedom required for the PML-based DtN, per element on the interfaces $\Sigma_{n,i}$ or $\Sigma_{n,i,j}$. Among the methods exhibiting the best convergence rate, the continuous approach are cheaper than the discontinuous discretization with polynomial degree $p + 1$. While in this 2D setting, the resulting difference in computational cost is not significant, it should be investigated further for 3D problems.

In the next sections, only the continuous discretization with the additional corner equation (called *selected continuous discretization*) and the discontinuous discretization with the higher polynomial degree and the penalty (called *selected discontinuous discretization*) are considered for the analyses.

For both selected discretizations, there is a sharp decay of the residual and the L_2-error between the third and the fourth GMRES iterations. This can be interpreted by considering that, at each iteration, information can be transferred only between neighboring subdomains. Given the considered domain partition and the position of the source in the lower left subdomain, four iterations are required to propagate the source accross all the subdomains. Because PML transmission conditions are particularly well-suited for this benchmark, the DDM solution is very close to the physical solution after only four iterations. Let us mention, that the relative error between the reference numerical solution (with any discretization) and the analytic solution (56) is equal to 6.8×10^{-3} for $p = 2$ and 6.3×10^{-3} for $p = 4$. These errors are higher that the relative errors observed between the DDM solutions and the reference solution after the four iterations.

4.3. Influence of the absorbing function in the transmission condition

Different absorbing functions can be used in the PMLs. Smoothly increasing functions such as polynomial and hyperbolic functions are frequently chosen. In this work, we consider quadratic, hyperbolic and shifted hyperbolic functions defined as

$$\sigma_q(x) = \sigma^\star (x - L_x)^2 \big/ \delta_{\text{PML}}^2, \tag{61}$$

$$\sigma_h(x) = 1 \big/ (\delta_{\text{PML}} - (x - L_x)), \tag{62}$$

$$\sigma_{hs}(x) = 1 \big/ (\delta_{\text{PML}} - (x - L_x)) - 1 \big/ \delta_{\text{PML}}, \tag{63}$$

respectively. These functions are written for a PML in the x-direction with $x \in [L_x, L_x + \delta_{\text{PML}}]$, like the last line in Equation (59). The definitions are similar for the other PMLs. In the quadratic function, the parameter $\sigma^\star$ must be tuned. Here, the values $\sigma^\star = 86.435$ and 186 have been used for $N_{\text{PML}} = 1$ and 6, respectively.

Figure 9 shows the convergence history of the DDM process when the PML transmission conditions are tested with the different absorbing functions, and PML thicknesses corresponding to $N_{\text{PML}} = 1$ (dashed lines) and 6 (plain lines). The computations are performed for both selected discretizations, and second-degree polynomial basis functions. In all the cases, the hyperbolic absorbing function and $N_{\text{PML}} = 6$ have been used for the PMLs on the exterior border of the global domain. Therefore, for a given discretization, the reference numerical solution remains the same.

We observe that, with six-cells PMLs in the transmission conditions, the convergence is similar with the different absorbing functions for each discretization. With one-cell PMLs, the convergence is slower in all the cases. The differences between the absorbing functions remain rather small in the discontinuous case, but they are significant in the continuous case. These observations can be related to the quality of the PML as a good absorbing boundary treatment. The accuracy of the technique is not very sensitive to the choice of the absorbing function with thick layers, but the choice is much more critical with very thin layers. Therefore, we can expect that the choice is not critical in the DDM procedure with thick layers. In the remainder, shifted hyperbolic functions are used for both exterior conditions and transmission conditions.

4.4. Influence of the PML thickness in the transmission condition

In order to study the influence of the PML thickness in the transmission conditions on the efficiency of the procedure, the convergence history with PML thicknesses corresponding to $N_{\text{PML}} = 1$, 2, 4 or 6 mesh cells is presented in Figure 10. The results obtained with the standard impedance transmission condition proposed by Després [20] are also presented (dashed lines). In all the cases, PMLs with $N_{\text{PML}} = 6$ are used for the exterior border of the global domain, and the shifted hyperbolic absorbing function is used for both PML-based transmission and boundary conditions. The selected continuous and discontinuous discretizations have been tested with second and fourth degree basis functions for the u-fields.

In all the cases, the relative residual and the relative L_2-error decrease with the number of iterations. They have approximately the same order of magnitude at each iteration. We observe that an increase of the

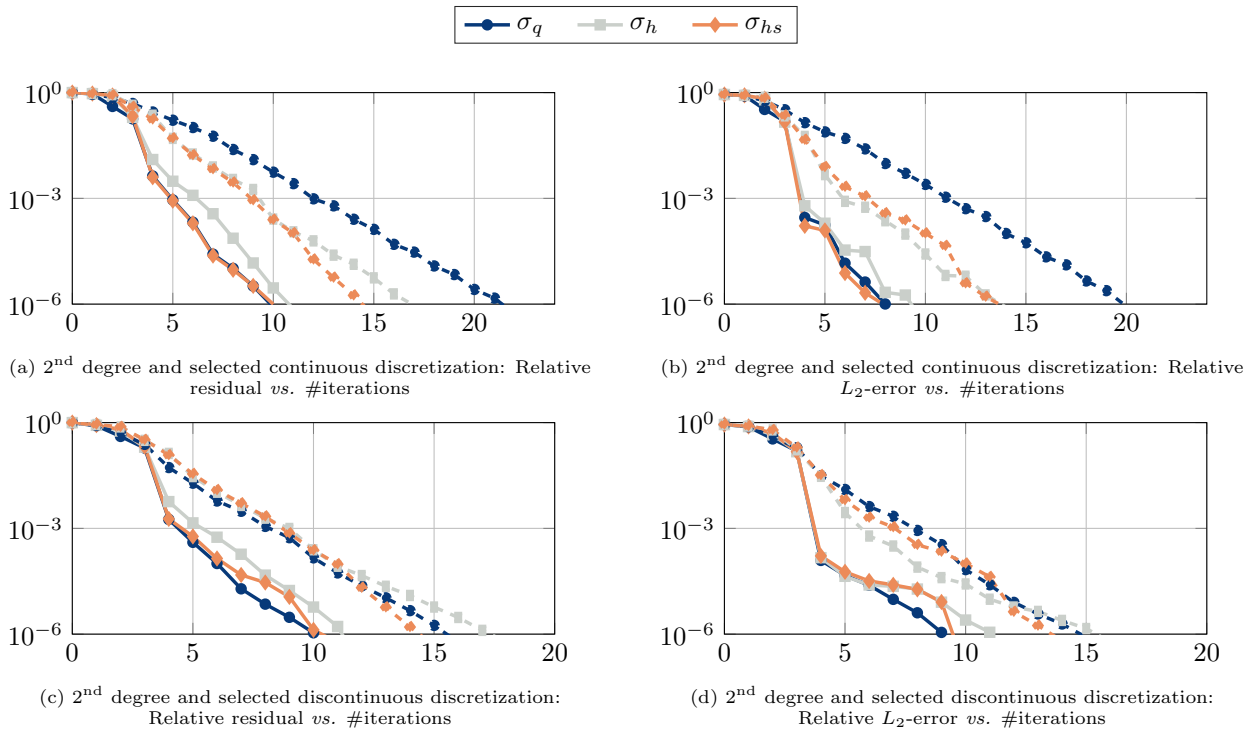

(a) 2nd degree and selected continuous discretization: Relative residual *vs.* #iterations

(b) 2nd degree and selected continuous discretization: Relative L_2-error *vs.* #iterations

(c) 2nd degree and selected discontinuous discretization: Relative residual *vs.* #iterations

(d) 2nd degree and selected discontinuous discretization: Relative L_2-error *vs.* #iterations

Figure 9: Convergence history of the second order PML-based DDM for different PML types. The dashed curves show the convergence history of the one-layer-size PMLs while the plain ones show the convergence history of the six-layer-size PMLs.

PML thickness accelerate the convergence of the DDM process up to a particular point where an increase of N_{PML} does not change the convergence rate anymore. The convergence is not much faster with the $N_{\text{PML}} = 6$ than with $N_{\text{PML}} = 4$. For the cheapest PML, with only one mesh cell in the thickness, the convergence is slower than with thicker PMLs, but it is much faster than with standard impedance transmission conditions. The results are similar with second and fourth degree basis functions.

4.5. Influence of the wavenumber and the mesh density

It is well known that the solution of high-frequency wave problems requires fine meshes with high-degree polynomial basis functions to decrease the dispersion error. Therefore, the efficiency of the solution procedures for large wavenumbers and fine meshes is a critical issue. Ideally, the influence the wavenumber and the mesh refinement on the convergence of the iterative procedure should be limited.

Figure 11 shows the number of GMRES iterations required to reach a relative residual lower than 10^{-6} as a function of the wavenumber k (left) and the mesh density $1/h$ (right). The computations are performed for a given mesh density (number of mesh vertices by wavelength equal to 15) in the first case, and for a given wavenumber ($k = 4\pi$) in the second case. The results are presented for PML-based transmission conditions with $N_{\text{PML}} = 1, 2, 4$ or 6, and second and fourth degree basis functions for the u-fields.

In all the cases, the number of GMRES iterations slightly increases with the wavenumber and the mesh density for very thin PMLs (*i.e.* with only one or two mesh cells in the thickness), while it remains very stable for thick PMLs. The resultats are similar for second and fourth degree basis functions. These results indicate that the PML-based transmission conditions are efficient for high-frequency scattering problems, as soon as the layers are sufficiently thick.

4.6. Benchmark with a smoothly varying heterogeneous medium

Finally, the DDM procedure is tested with a spatially varying medium, though it is a priori designed for problems with a constant wavenumber. The analysis is carried out with the Marmousi model shown

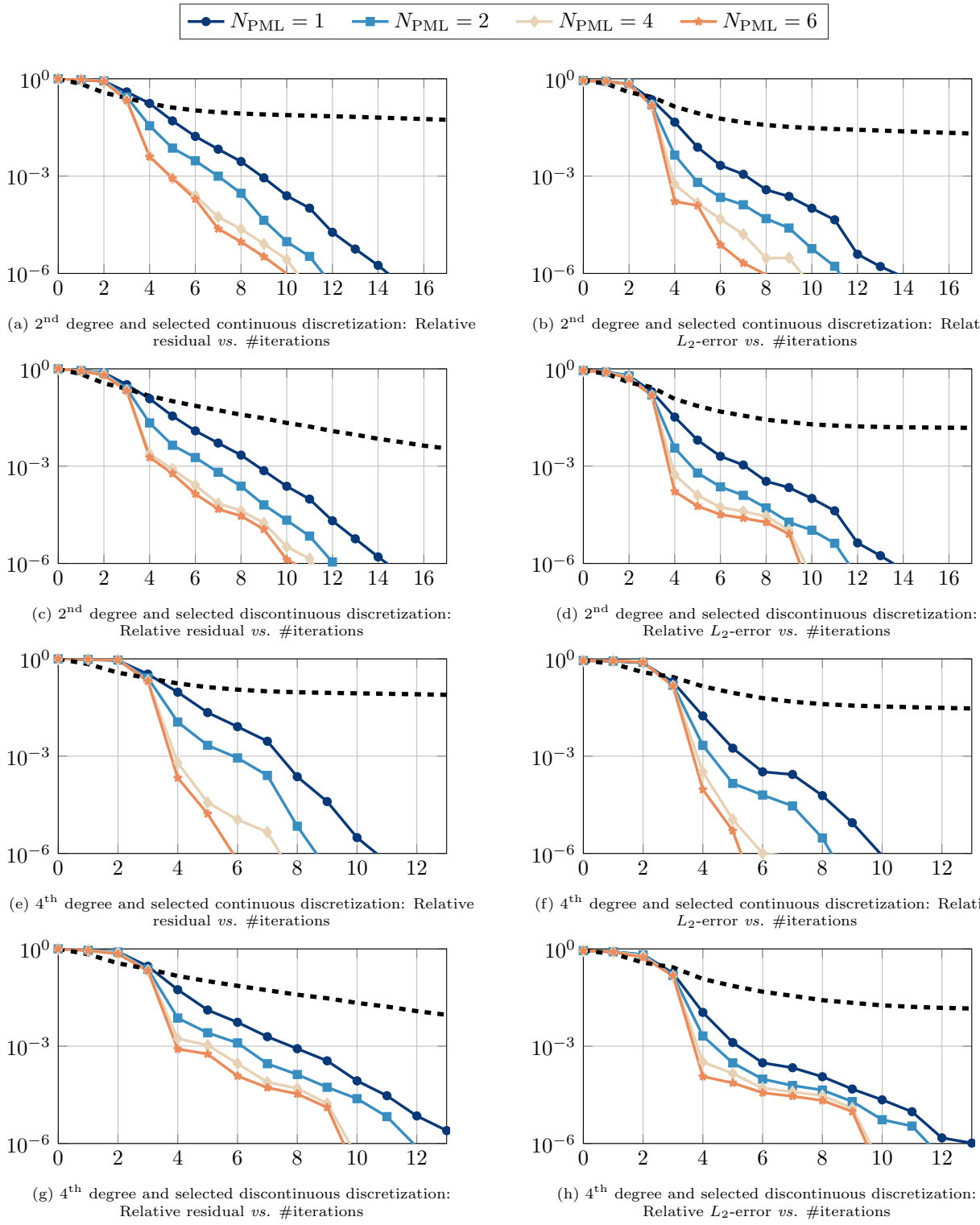

(a) 2nd degree and selected continuous discretization: Relative residual *vs.* #iterations

(b) 2nd degree and selected continuous discretization: Relative L_2-error *vs.* #iterations

(c) 2nd degree and selected discontinuous discretization: Relative residual *vs.* #iterations

(d) 2nd degree and selected discontinuous discretization: Relative L_2-error *vs.* #iterations

(e) 4th degree and selected continuous discretization: Relative residual *vs.* #iterations

(f) 4th degree and selected continuous discretization: Relative L_2-error *vs.* #iterations

(g) 4th degree and selected discontinuous discretization: Relative residual *vs.* #iterations

(h) 4th degree and selected discontinuous discretization: Relative L_2-error *vs.* #iterations

Figure 10: History of the relative GMRES residual (left) and the relative mono-domain L_2-error for different basis function orders and different number of layers in the PML. The dashed black curve corresponds to the results obtained when a 0th order transmission condition is imposed on interface edges while a six-layer-size PML is still imposed on the boundary edges of the domain (the reference problem).

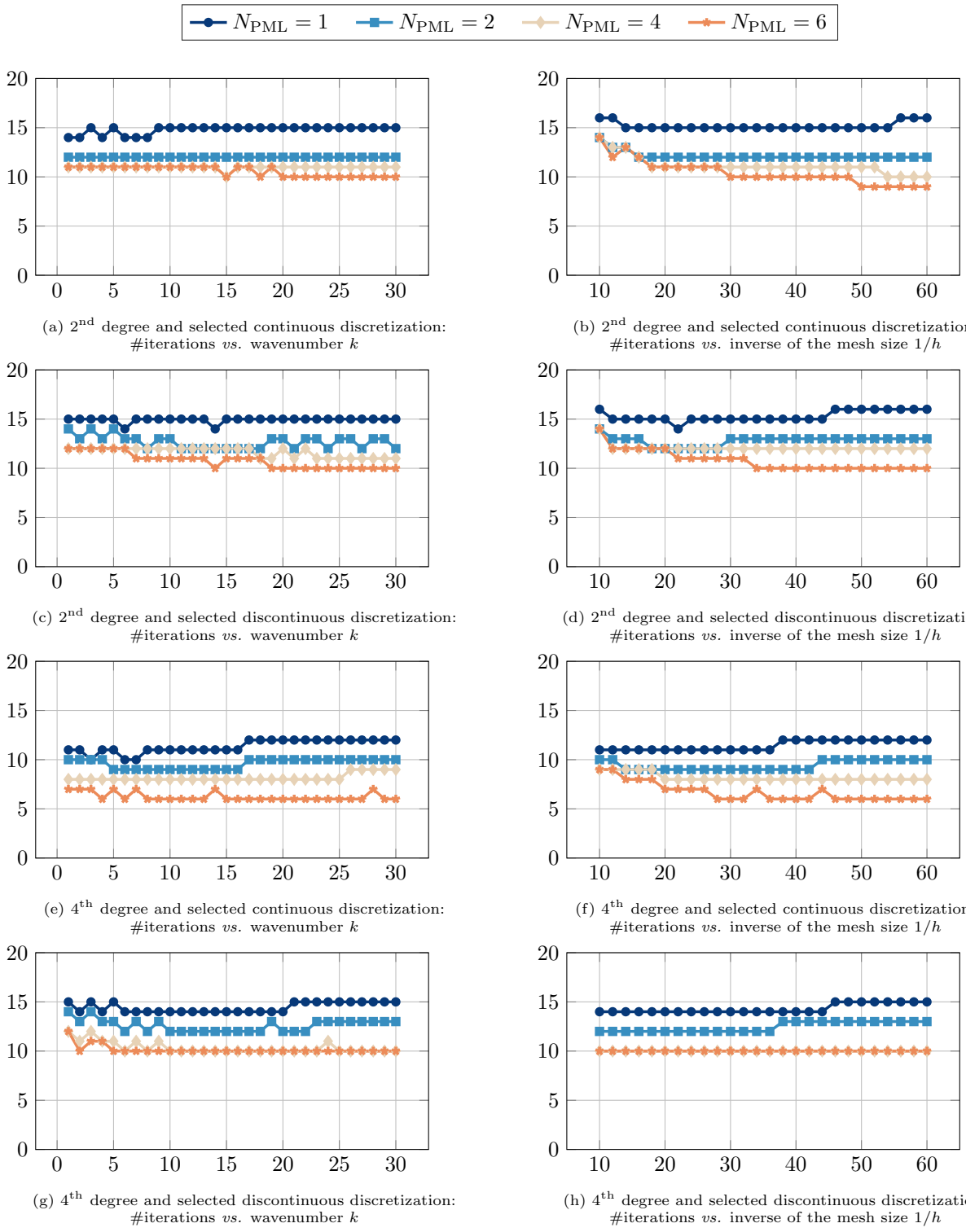

(a) 2nd degree and selected continuous discretization: #iterations *vs.* wavenumber k

(b) 2nd degree and selected continuous discretization: #iterations *vs.* inverse of the mesh size $1/h$

(c) 2nd degree and selected discontinuous discretization: #iterations *vs.* wavenumber k

(d) 2nd degree and selected discontinuous discretization: #iterations *vs.* inverse of the mesh size $1/h$

(e) 4th degree and selected continuous discretization: #iterations *vs.* wavenumber k

(f) 4th degree and selected continuous discretization: #iterations *vs.* inverse of the mesh size $1/h$

(g) 4th degree and selected discontinuous discretization: #iterations *vs.* wavenumber k

(h) 4th degree and selected discontinuous discretization: #iterations *vs.* inverse of the mesh size $1/h$

Figure 11: Number of GMRES iterations needed to reach the relative residual of 10^{-6} as a function of the wavenumber k with a constant number of point by wavelength of 15 (left graphs) and as a function of the inverse of the characteristic mesh size $1/h$ with a fixed wavenumber $k = 4\pi$ (right graphs), for different basis function orders and different number of layers in the interface PML. The dashed black curves correspond to the results obtained when a 0th order transmission condition is imposed on interface edges while the six-layer-size PML is imposed on the boundary edges of the domain (the reference problem).

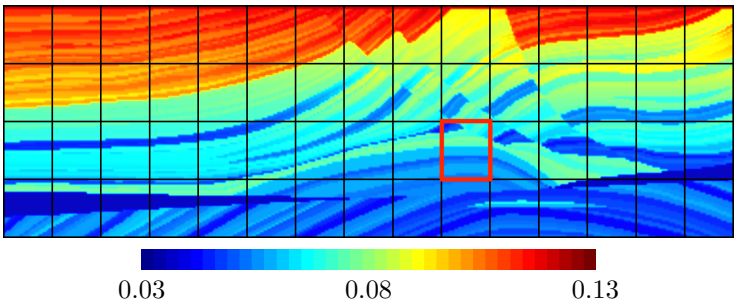

(a) Wavenumber distribution

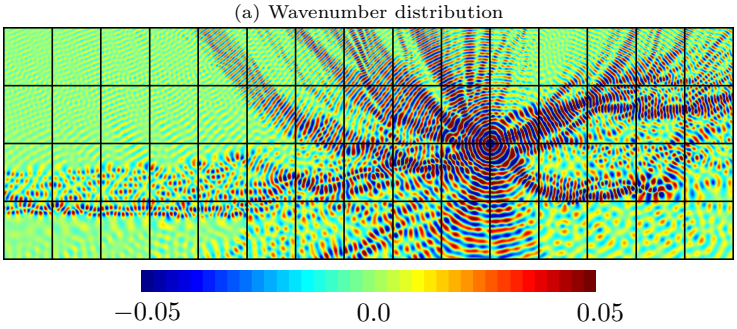

(b) Real part of the numerical solution

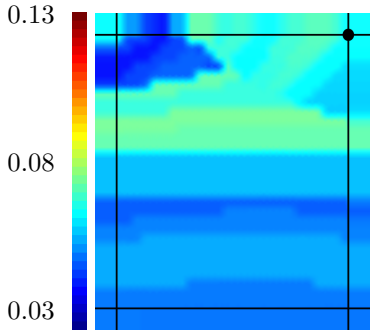

(c) Material parameters in PMLs surrounding the subdomain with the source point

Figure 12: Marmousi benchmark: wavenumber distribution (a), numerical solution (b) and subdomain where the source is prescribed (c). One can notice the extruded wavenumber inside the surrounded PMLs.

in Figure 12a, which represents a realistic geological structure. The spatially varying wavenumber is given by $k(\mathbf{x}) = 2\pi f/\nu(\mathbf{x})$ with the velocity map $\nu(\mathbf{x})$ and the frequency $f = 30$Hz. The rectangular domain $\Omega_{\text{glo}} = [0, 9192\text{ m}] \times [-2904\text{ m}, 0]$ is surrounded with PMLs. A point source is located at the position $\mathbf{x}_{\text{s}}$, leading to the following Helmholtz equation

$$-\Delta u - k(\mathbf{x})^2 u = \delta(\mathbf{x} - \mathbf{x}_{\text{s}}), \quad \text{on } \Omega_{\text{glo}}, \tag{64}$$

where δ is the Dirac delta function. The domain is meshed with rectangular elements of characteristic size $h \approx 10\,\text{m}$. First-degree basis functions are used for the u-fields.

The domain is partitioned into a checkerboard grid of 15×4 subdomains, as depicted in Figure 12a. Each subdomain is composed of 4588 rectangular elements. The source term is placed at a cross-point in order to demonstrate the flexibility of the method. In practice, it is taken into account by only one subdomain touching this cross-point to ensure the equivalence with the original problem. The method is tested with PML thicknesses equal to $N_{\text{PML}} = 1$, 2 and 3 mesh cells in the transmission conditions, and equal to $N_{\text{PML}} = 6$ for the exterior boundary condition. Because the wavenumber is not constant, a strategy must be chosen to define the wavenumber in the PMLs. Inside the edge PMLs, the value of the wavenumber is simply extruded from the interface with the subdomain, then it does not vary in the tangential direction. Inside the corner PMLs, the wavenumber is constant, equal to the value at the corresponding corner of the subdomain. Figure 12c illustrates the wavenumber for the subdomain where the source term is prescribed.

The convergence history for the relative residual is shown on Figure 13 for both continuous and discontinuous discretizations. In all the cases, the final relative L^2-error between the DDM solution and the reference numerical solution is close to 10^{-6}. We observe on Figure 13 that the DDM procedure is much faster with PML transmission conditions (even with the thinnest PMLs) than with the standard impedance transmission conditions (dashed curves). Increasing the thickness of the PML accelerate the convergence for both discretizations, but the efficiency is not much better when increasing the thickness from 2 to 3 mesh cells.

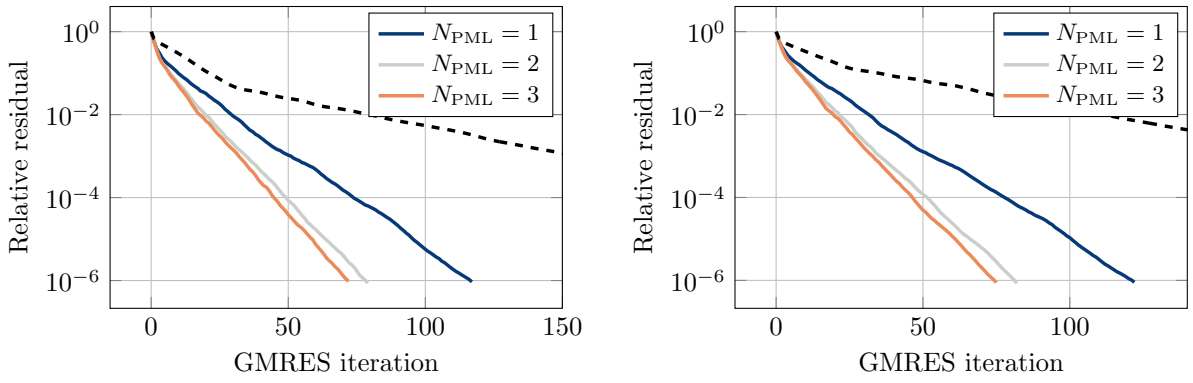

(a) Selected continuous discretization

(b) Selected discontinuous discretization

Figure 13: Marmousi benchmark. Convergence history with the PML transmissions conditions. The dashed curve corresponds to the results obtained with the standard impedance transmission condition.

5. Conclusions and perspectives

We have proposed a non-overlapping DDM with PML transmission conditions for the Helmholtz equation. Our approach naturally takes into account cross-points for two-dimensional checkerboard domain partitions. It relies on Lagrange multipliers used for the weak coupling between subproblems defined on the rectangular subdomains and the surrounding PMLs. They are also used to compute the transmission variables for the DDM procedure. Two discretizations for the Lagrange multipliers and several stabilization strategies were compared. The best two converging approaches are the continuous discretization with additional corner equation, and the discontinuous discretization with higher polynomial degree and penalty. In addition to convergence rates, selecting the best approach among all presented discretizations and stabilization strategies might however depend on the user's software implementation and accuracy requirements. Indeed, $\mathbf{H}(\text{div})$-conforming basis functions might not be implemented in all finite element codes; and adding corner treatments requires geometrical identifications and algebraic constraints that could be more or less straightforward to deal with depending on the computational framework.

The extension to three-dimensional problems is clearly possible, but special attention will need to be paid to the stability of the discretizations. The extension to other physical contexts such as electromagnetics, electrodynamics or flow acoustics should be fairly straightforward as well, since PML formulations already exist for these problems.

Acknowledgments

This research was funded in part through the ARC grant for Concerted Research Actions (ARC WAVES 15/19-03), financed by the Wallonia-Brussels Federation of Belgium.

Computational resources have been provided by the Consortium des Équipements de Calcul Intensif (CÉCI), funded by the Fonds de la Recherche Scientifique de Belgique (F.R.S.-FNRS) under Grant No. 2.5020.11 and by the Walloon Region.

References

[1] A. V. Astaneh and M. N. Guddati. A two-level domain decomposition method with accurate interface conditions for the Helmholtz problem. *International Journal for Numerical Methods in Engineering*, 107(1):74–90, 2016.

[2] K.-J. Bathe. The inf-sup condition and its evaluation for mixed finite element methods. *Computers and Structures*, pages 1–10, Sept. 2000.

[3] É. Béchet, N. Moës, and B. I. Wohlmuth. A stable Lagrange multiplier space for stiff interface conditions within the extended finite element method. *International Journal for Numerical Methods in Engineering*, 78(8):931–954, May 2009.

[4] J.-D. Benamou and B. Desprès. A domain decomposition method for the Helmholtz equation and related optimal control problems. *Journal of Computational Physics*, 136(1):68–82, 1997.

[5] A. Bendali and Y. Boubendir. Non-overlapping domain decomposition method for a nodal finite element method. *Numerische Mathematik*, 103(4):515–537, 2006.

[6] A. Bermúdez, L. Hervella-Nieto, A. Prieto, and R. Rodríguez. An exact bounded pml for the Helmholtz equation. *Comptes Rendus Mathematique*, 339(11):803–808, Dec. 2004.

[7] A. Bermúdez, L. Hervella-Nieto, A. Prieto, and R. Rodríguez. An optimal perfectly matched layer with unbounded absorbing function for time-harmonic acoustic scattering problems. *Journal of Computational Physics*, 223(2): 469–488, May 2007.

[8] A. Bermúdez, L. Hervella-Nieto, A. Prieto, and R. Rodríguez. An exact bounded perfectly matched layer for time-harmonic scattering problems. *SIAM Journal on Scientific Computing*, 30(1):312–338, Dec. 2007.

[9] D. Boffi, F. Brezzi, and M. Fortin. *Mixed Finite Element Methods and Applications*, volume 44. Springer, 2013.

[10] Y. Boubendir and D. Midura. Non-overlapping domain decomposition algorithm based on modified transmission conditions for the Helmholtz equation. *Computers & Mathematics with Applications*, 75(6):1900–1911, 2018.

[11] Y. Boubendir, X. Antoine, and C. Geuzaine. A quasi-optimal non-overlapping domain decomposition algorithm for the Helmholtz equation. *Journal of Computational Physics*, 231(2):262 – 280, 2012.

[12] X.-C. Cai and O. B. Widlund. Domain decomposition algorithms for indefinite elliptic problems. *SIAM Journal on Scientific and Statistical Computing*, 13(1):243–258, 1992.

[13] X. Claeys. Non-local variant of the optimised schwarz method for arbitrary non-overlapping subdomain partitions. *ESAIM: M2AN*, 55(2):429–448, 2021. doi: 10.1051/m2an/2020083.

[14] X. Claeys and E. Parolin. Robust treatment of cross points in optimized Schwarz methods, 2020. Preprint. http://arxiv.org/abs/2003.06657.

[15] X. Claeys, F. Collino, and E. Parolin. Matrix form of nonlocal OSM for electromagnetics, 2021. Preprint. http://arxiv.org/abs/2108.11352.

[16] F. Collino, S. Ghanemi, and P. Joly. Domain decomposition method for harmonic wave propagation: a general presentation. *Computer Methods in Applied Mechanics and Engineering*, 184(2-4):171–211, 2000.

[17] F. Collino, P. Joly, and M. Lecouvez. Exponentially convergent non overlapping domain decomposition methods for the Helmholtz equation. *ESAIM: Mathematical Modelling and Numerical Analysis*, 54(3):775–810, 2020.

[18] L. Conen, V. Dolean, R. Krause, and F. Nataf. A coarse space for heterogeneous Helmholtz problems based on the Dirichlet-to-Neumann operator. *Journal of Computational and Applied Mathematics*, 271:83–99, 2014.

[19] A. de La Bourdonnaye, C. Farhat, A. Macedo, F. Magoules, and F.-X. Roux. A non-overlapping domain decomposition method for the exterior helmhokz problem. *Contemporary Mathematics*, 218:42–66, 1998.

[20] B. Després. *Méthodes de décomposition de domaines pour les problemes de propagation d'ondes en régime harmonique. Le théoreme de Borg et l'équation de Hill vectorielle*. PhD thesis, Ph. D. dissertation, Université Paris 9, France, 1991.

[21] B. Després, A. Nicolopoulos, and B. Thierry. Corners and stable optimized domain decomposition methods for the Helmholtz problem, May 2020. Preprint. https://hal.archives-ouvertes.fr/hal-02612368.

[22] B. Després, A. Nicolopoulos, and B. Thierry. On domain decomposition methods with optimized transmission conditions and cross-points, May 2021. Preprint. https://hal.archives-ouvertes.fr/hal-03230250.

[23] A. Ern and J.-L. Guermond. *Finite Elements II, Galerkin Approximation, Elliptic and Mixed PDEs*, chapter 50, page 364. Texts in Applied Mathematics. Springer, Cham, 2021.

[24] O. G. Ernst and M. J. Gander. Why it is difficult to solve Helmholtz problems with classical iterative methods. *Numerical analysis of multiscale problems*, pages 325–363, 2012.

[25] C. Farhat, A. Macedo, and M. Lesoinne. A two-level domain decomposition method for the iterative solution of high frequency exterior Helmholtz problems. *Numerische Mathematik*, 85(2):283–308, 2000.

[26] C. Farhat, A. Macedo, M. Lesoinne, F.-X. Roux, F. Magoulés, and A. de La Bourdonnaie. Two-level domain decomposition methods with Lagrange multipliers for the fast iterative solution of acoustic scattering problems. *Computer Methods in Applied Mechanics and Engineering*, 184(2-4):213–239, 2000.

[27] C. Farhat, P. Avery, R. Tezaur, and J. Li. FETI-DPH: a dual-primal domain decomposition method for acoustic scattering. *Journal of Computational Acoustics*, 13:499–524, 2005.

[28] M. J. Gander and L. Halpern. A simple finite difference discretization for Ventcell transmission conditions at cross points. In *Proceedings of the 26th International Domain Decomposition Conference*. 2020.

[29] M. J. Gander and K. Santugini-Repiquet. Cross-points in domain decomposition methods with a finite element discretization. *Electronic Transactions on Numerical Analysis*, 45:219–240, 2016.

[30] M. J. Gander and H. Zhang. Optimized Schwarz methods with overlap for the Helmholtz equation. *SIAM Journal on Scientific Computing*, 38(5):A3195–A3219, 2016.

[31] M. J. Gander and H. Zhang. A class of iterative solvers for the Helmholtz equation: Factorizations, sweeping preconditioners, source transfer, single layer potentials, polarized traces, and optimized Schwarz methods. *SIAM Review*, 61(1):3–76, 2019.

[32] M. J. Gander, F. Magoules, and F. Nataf. Optimized Schwarz methods without overlap for the Helmholtz equation. *SIAM Journal on Scientific Computing*, 24(1):38–60, 2002.

[33] M. Ganesh and C. Morgenstern. High-order FEM domain decomposition models for high-frequency wave propagation in heterogeneous media. *Computers & Mathematics with Applications*, 75(6):1961–1972, 2018.

[34] C. Geuzaine and J.-F. Remacle. Gmsh: A 3-D finite element mesh generator with built-in pre- and post-processing facilities. *International Journal for Numerical Methods in Engineering*, 79:1309–1331, May 2009.

[35] I. Graham, E. Spence, and E. Vainikko. Domain decomposition preconditioning for high-frequency Helmholtz problems with absorption. *Mathematics of Computation*, 86(307):2089–2127, 2017.

[36] T. Hagstrom, R. P. Tewarson, and A. Jazcilevich. Numerical experiments on a domain decomposition algorithm for nonlinear elliptic boundary value problems. *Applied Mathematics Letters*, 1(3):299–302, 1988.

[37] S. Kim and H. Zhang. Optimized Schwarz method with complete radiation transmission conditions for the Helmholtz equation in waveguides. *SIAM Journal on Numerical Analysis*, 53(3):1537–1558, 2015.

[38] J.-H. Kimn and M. Sarkis. Restricted overlapping balancing domain decomposition methods and restricted coarse problems for the Helmholtz problem. *Computer Methods in Applied Mechanics and Engineering*, 196(8): 1507–1514, 2007.

[39] M. Lecouvez. *Méthodes itératives de décomposition de domaine sans recouvrement avec convergence géométrique pour l'équation de Helmholtz*. PhD thesis, École Polytechnique, 2015.

[40] M. Lecouvez, B. Stupfel, P. Joly, and F. Collino. Quasi-local transmission conditions for non-overlapping domain decomposition methods for the Helmholtz equation. *Comptes Rendus Physique*, 15(5):403–414, 2014.

[41] W. Leng and L. Ju. An additive overlapping domain decomposition method for the Helmholtz equation. *SIAM Journal on Scientific Computing*, 41(2):A1252–A1277, 2019.

[42] N. Marsic and H. De Gersem. Convergence of classical optimized non-overlapping Schwarz method for Helmholtz problems in closed domains, 2021. Preprint. http://arxiv.org/abs/2001.01502.

[43] A. Modave, C. Geuzaine, and X. Antoine. Corner treatments for high-order local absorbing boundary conditions in high-frequency acoustic scattering. *Journal of Computational Physics*, 401:109029, 2020.

[44] A. Modave, A. Royer, X. Antoine, and C. Geuzaine. A non-overlapping domain decomposition method with high-order transmission conditions and cross-point treatment for Helmholtz problems. *Computer Methods in Applied Mechanics and Engineering*, 368:113162, 2020.

[45] A. Moiola and E. A. Spence. Is the Helmholtz equation really sign-indefinite? *SIAM Review*, 56(2):274–312, 2014.

[46] F. Nataf. Interface connections in domain decomposition methods. In *Modern methods in scientific computing and applications*, pages 323–364. Springer, 2002.

[47] F. Nataf and F. Nier. Convergence rate of some domain decomposition methods for overlapping and nonoverlapping subdomains. *Numerische Mathematik*, 75(3):357–377, 1997.

[48] F. Nataf, F. Rogier, and E. de Sturler. Optimal interface conditions for domain decomposition methods. *CMAP (Ecole Polytechnique)*, 301:1–18, 1994.

[49] J.-C. Nédélec. Mixed finite elements in $\mathbb{R}^3$. *Numerische Mathematik*, 35:315–341, 1980.

[50] J.-C. Nédélec. A new family of mixed finite elements in $\mathbb{R}^3$. *Numerische Mathematik*, 50:57–81, 1986.

[51] A. Nicolopoulos-Salle. *Formulations variationnelles d'équations de Maxwell résonantes et problèmes aux coins en propagation d'ondes*. PhD thesis, Sorbonne université, 2019.

[52] É. Parolin. *Non-overlapping domain decomposition methods with non-local transmissionoperators for harmonic*

wave propagation problems. PhD thesis, Institut Polytechnique de Paris, 2020.

[53] Z. Peng and J.-F. Lee. Non-conformal domain decomposition method with second-order transmission conditions for time-harmonic electromagnetics. *Journal of Computational Physics*, 229(16):5615–5629, 2010.

[54] A. Piacentini and N. Rosa. An improved domain decomposition method for the 3D Helmholtz equation. *Computer Methods in Applied Mechanics and Engineering*, 162(1-4):113–124, 1998.

[55] A. Royer, É. Béchet, and C. Geuzaine. Gmsh-Fem: An efficient finite element library based on Gmsh. In *14th WCCM-ECCOMAS Congress*, pages 1–13, Mar. 2021.

[56] A. Schädle and L. Zschiedrich. Additive Schwarz method for scattering problems using the pml method at interfaces. In *Domain decomposition methods in science and engineering XVI*, pages 205–212. Springer, 2007.

[57] P. Solin, K. Segeth, and I. Dolezel. *Higher-Order Finite Element Methods*. CRC Press, 2003.

[58] C. C. Stolk. A rapidly converging domain decomposition method for the Helmholtz equation. *Journal of Computational Physics*, 241:240–252, 2013.

[59] C. C. Stolk. An improved sweeping domain decomposition preconditioner for the Helmholtz equation. *Advances in Computational Mathematics*, 43(1):45–76, 2017.

[60] B. Stupfel. Improved transmission conditions for a one-dimensional domain decomposition method applied to the solution of the Helmholtz equation. *Journal of Computational Physics*, 229(3):851–874, 2010.

[61] B. Thierry, A. Vion, S. Tournier, M. El Bouajaji, D. Colignon, N. Marsic, X. Antoine, and C. Geuzaine. GetDDM: An open framework for testing optimized Schwarz methods for time-harmonic wave problems. *Computer Physics Communications*, 203:309–330, 2016.

[62] A. Toselli. Some results on overlapping Schwarz methods for the Helmholtz equation employing perfectly matched layers. In *Domain Decomposition Methods in Sciences and Engineering XI*, pages 539–545, 1998.

[63] A. Toselli and O. Widlund. *Domain Decomposition Methods - Algorithms and Theory*, volume 34. Springer-Verlag Berlin Heidelberg, 2005.

[64] A. Vion and C. Geuzaine. Double sweep preconditioner for optimized Schwarz methods applied to the Helmholtz problem. *Journal of Computational Physics*, 266:171–190, 2014.

[65] L. Zepeda-Núñez and L. Demanet. The method of polarized traces for the 2D Helmholtz equation. *Journal of Computational Physics*, 308:347–388, 2016.

[66] L. Zepeda-Núñez, A. Scheuer, R. J. Hewett, and L. Demanet. The method of polarized traces for the 3D Helmholtz equation. *Geophysics*, 84(4):T313–T333, 2019.